

# Projected Changes in Future Extreme Precipitation over the Northeast US in the NA-CORDEX Ensemble

Robert Nazarian<sup>1,1,1</sup>, James Vizzard<sup>1,1,1</sup>, Carissa Agostino<sup>1,1,1</sup>, and Nicholas Lutsko<sup>2,2,2</sup>

<sup>1</sup>Fairfield University

<sup>2</sup>Scripps Institution of Oceanography

November 30, 2022

## Abstract

The northeast United States (NEUS) is a densely-populated region with a number of major cities along the climatological storm track. Despite its economic and social importance, as well as the area's vulnerability to flooding, there is significant uncertainty regarding future trends in extreme precipitation over the region. Here, we undertake a regional study of the projected changes in extreme precipitation over the NEUS, measured with a variety of metrics, through the end of the 21st century in an ensemble of high-resolution, dynamically-downscaled simulations from the NA-CORDEX project. We find that extreme precipitation increases throughout the region, with the largest changes in coastal regions and smaller increases inland. These increases are seen throughout the year, though the smallest changes in extreme precipitation are seen in the spring. The frequency of heavy precipitation also increases, such that there are relatively fewer days with moderate precipitation and relatively more days with either no or strong precipitation. Averaged over the region, extreme precipitation increases by +3-4%/°C of local warming, with the largest fractional increases in southern and inland regions. This is lower than the +7%/°C rate expected from thermodynamic considerations alone, and suggests that dynamical changes damp the increases in extreme precipitation. These changes are qualitatively robust across ensemble members, though there is notable intermodel spread associated with models' climate sensitivity and with changes in mean precipitation. Together, the NA-CORDEX simulations suggest that this densely populated region may require significant adaptation strategies to cope with the increase in extreme precipitation expected at the end of the next century.

**Projected Changes in Future Extreme Precipitation over the  
Northeast US in the NA-CORDEX Ensemble**

Robert H. Nazarian,<sup>a</sup> James V. Vizzard,<sup>a</sup> Carissa P. Agostino,<sup>a</sup> and Nicholas J. Lutsko,<sup>b</sup>

<sup>a</sup> *Department of Physics, Fairfield University, Fairfield CT, USA*

<sup>b</sup> *Scripps Institution of Oceanography, University of California at San Diego, La Jolla,  
CA, USA*

*Corresponding author:* Robert H. Nazarian, rnazarian@fairfield.edu

This work has been submitted to the Journal of Applied Meteorology and Climatology.

Copyright in this work may be transferred without further notice.



10 ABSTRACT: The northeast United States is a densely-populated region with a number  
11 of major cities along the climatological storm track. Despite its economic and social  
12 importance, as well as the area's vulnerability to flooding, there is significant uncertainty  
13 regarding future trends in extreme precipitation over the region. Here, we undertake a  
14 regional study of the projected changes in extreme precipitation over the NEUS through  
15 the end of the 21st century using an ensemble of high-resolution, dynamically-downscaled  
16 simulations from the NA-CORDEX project. We find that extreme precipitation increases  
17 throughout the region, with the largest changes in coastal regions and smaller changes  
18 inland. These increases are seen throughout the year, though the smallest changes in  
19 extreme precipitation are seen in the summer, in contrast to earlier studies. The frequency  
20 of heavy precipitation also increases, such that there are relatively fewer days with moderate  
21 precipitation and relatively more days with either no or strong precipitation. Averaged  
22 over the region, extreme precipitation increases by +3-5%/°C of local warming, with the  
23 largest fractional increases in southern and inland regions, and occurring during the winter  
24 and spring seasons. This is lower than the +7%/°C rate expected from thermodynamic  
25 considerations alone, and suggests that dynamical changes damp the increases in extreme  
26 precipitation. These changes are qualitatively robust across ensemble members, though  
27 there is notable intermodel spread associated with models' climate sensitivity and with  
28 changes in mean precipitation. Together, the NA-CORDEX simulations suggest that this  
29 densely populated region may require significant adaptation strategies to cope with the  
30 increase in extreme precipitation expected at the end of the next century.

SIGNIFICANCE STATEMENT: Observations show that the northeast United States has already experienced increases in extreme precipitation, and prior modeling studies suggest that this trend is expected to continue through the end of the century. Using high-resolution climate model simulations, we find that coastal regions will experience large increases in extreme precipitation (+6.0-7.5 mm/day), although there is significant intermodel spread in the trends' spatial distribution as well as in their seasonality. Regionally-averaged, extreme precipitation will increase at a rate of roughly 2%/decade. Our results also suggest that the frequency of extreme precipitation will increase, with the strongest storms doubling in frequency per degree warming. These results, taken with earlier studies, provide guidance to aid in resiliency preparation and planning by regional stakeholders.

## 1. Introduction

Changes in extreme precipitation have the potential to be among the most damaging impacts of global warming, with significant ramifications for agriculture (Rosenzweig et al. 2002), severe flooding (Tabari 2020), and landslides (Kirschbaum et al. 2012), among many other things. Observations show that global-mean extreme precipitation has increased in intensity and frequency throughout the globe over the past century (Groisman et al. 2005; Alexander et al. 2006) and numerous modeling studies suggest extreme precipitation will continue to change as the climate warms (Kao and Ganguly 2011; Fischer et al. 2013; Kharin et al. 2013; Fischer et al. 2014; O’Gorman 2015; Bao et al. 2017). The magnitude of this change, however, is regionally- and model-dependent. Understanding the extent to which extreme precipitation will change through the end of the century is vitally important as communities look to develop resilience to extreme precipitation and associated flooding events (Wilhelmi and Morss 2013; Gandini et al. 2020).

In the present study, we focus on extreme precipitation trends in the northeast United States (hereafter NEUS). This region is of particular interest due to its high population density, coupled with the distribution of large cities along the climatological storm tracks (Kocin and Uccellini 2004; Zarzycki 2018). Observational studies have shown that extreme

precipitation over the NEUS has increased by approximately 2-4%/decade over the past century, depending on the observational product and on the mode of analysis (Kunkel and et al. 2013; Agel et al. 2015; Frei et al. 2015; Ivancic and Shaw 2016; Hoerling et al. 2016; Huang et al. 2017; Agel et al. 2018; Huang et al. 2018; Howarth et al. 2019; Lopez-Cantu et al. 2020). These trends show substantial seasonality, with the largest increases in the warm season [i.e. June, July, August, and September] (Frei et al. 2015).

Several modeling studies have provided comparisons with observations and diagnosed potential mechanisms for the increases in precipitation (Hoerling et al. 2016; Agel et al. 2020; Agel and Barlow 2020; Huang et al. 2021). These simulations have shown relatively good agreement with observations of extreme precipitation in terms of magnitude and seasonality, and have also found that resolution is of first-order importance for accurately capturing the spatial distribution of extreme precipitation. Interestingly, there is little difference in the performance of the CMIP5 and CMIP6 ensembles in the region (Agel et al. 2020; Agel and Barlow 2020), suggesting that improvements to model physics have not resulted in improved representations of the NEUS climate.

Modeling studies of future extreme precipitation over the NEUS are more limited. Sheffield et al. (2013) and Sillmann et al. (2013) evaluated CMIP5 output at the regional scale and found that, while there is some agreement in the sign of the trend in extreme precipitation over the NEUS, the magnitude differs notably between models. Furthermore, the simulated precipitation was shown to be biased low due to the coarse resolution of the models. Thibeault and Seth (2014) analyzed the CMIP5 ensemble and found that the projected increases in total annual precipitation are driven by increases in winter extreme precipitation, in contrast with the observations of Frei et al. (2015). Additionally, Thibeault and Seth (2014) found that the largest changes are projected in coastal and northern portions of the NEUS.

Hayhoe et al. (2008) and Rawlins et al. (2012) used Regional Climate Models (RCMs) to analyze future mean and extreme precipitation in the NEUS, with both studies reporting the largest increase in winter months, as well as a coastal enhancement of precipitation.

86 However, Hayhoe et al. (2008) analyzed monthly-averaged data, which is too low resolution  
87 to use for adaptation and planning purposes, and only three models were considered, with a  
88 relatively narrow range in climate sensitivities. Similarly, the results of Rawlins et al. (2012)  
89 were presented as seasonal values, and only extended to the mid-21st century. Ning et al.  
90 (2015) and Wang et al. (2020) used two independent, statistically-downscaled ensembles  
91 to study extreme precipitation over the region and found consistent spatial patterns of  
92 change but very different magnitudes, as well as differences in the frequency of extreme  
93 precipitation. Finally, Ashfaq et al. (2016) and Rastogi et al. (2020) used an ensemble  
94 of CMIP5 simulations downscaled over the United States and showed that the number of  
95 extreme precipitation days that the NEUS experiences are expected to increase by mid-  
96 century.

97 Given the relatively limited number of modeling studies of, future NEUS extreme precip-  
98 itation trends, as well as the importance of resolution for accurately simulating precipitation  
99 in the region, there is an urgent need for studies of future trends in NEUS extreme pre-  
100 cipitation using high resolution climate model simulations. More generally, several recent  
101 studies have shown that dynamically-downscaling GCM simulations using high resolution  
102 RCMs can provide “added value” in capturing smaller-scaled climate processes compared  
103 to using only GCMs (Diffenbaugh et al. 2005; Di Luca et al. 2012; Ashfaq et al. 2016;  
104 Lucas-Picher et al. 2016), as RCMs capture a greater number of the mesoscale phenomena  
105 that lead to extreme precipitation. RCMs also afford more realistic representations of sur-  
106 face forcing [such as orography] (Leung et al. 2003) and of the atmosphere’s circulation,  
107 both of which contribute to more realistic projections of extreme precipitation [although  
108 both GCMs and RCMs have been shown to poorly capture extreme precipitation due to  
109 convection (O’Gorman 2015; Muller and Takayabu 2020)].

110 With this motivation, in the present study we examine projected trends in extreme pre-  
111 cipitation over the NEUS in the COordinated Regional climate Downscaling EXperiment  
112 (CORDEX). CORDEX consists of dynamically-downscaled GCM simulations, designed  
113 using the CMIP5 GCM ensemble, and serves to evaluate and improve regional climate

114 downscaling models and techniques, as well as to explore regional climate processes. To  
115 study trends in extreme precipitation in the NEUS, we use the NA-CORDEX ensemble,  
116 which provides downscaled simulations over the North American region. The ensemble  
117 members in NA-CORDEX sample nearly the entire range of climate sensitivity in CMIP5  
118 (Bukovsky and Mearns 2020), and thus can be expected to provide a realistic representation  
119 of model uncertainty in future warming. In contrast, the ensembles of driving GCMs used  
120 in prior studies of future trends over the NEUS had significantly narrower ranges of cli-  
121 mate sensitivity. Furthermore, NA-CORDEX uses the CMIP5 ensemble whereas previous  
122 studies, such as Rawlins et al. (2012), were based on an older generation of models used  
123 in the North American Regional Climate Change Assessment Program. The mean state of  
124 the NA-CORDEX simulations has been previously analyzed by Lucas-Picher et al. (2016);  
125 Karmalkar (2018); Bukovsky and Mearns (2020), and uncertainty in extreme precipitation  
126 over the NA-CORDEX domain was briefly discussed by Lopez-Cantu et al. (2020) in a  
127 larger study of extreme precipitation projections over the continental United States. A de-  
128 tailed analysis of trends in both annual and seasonal extreme precipitation over the NEUS  
129 in the NA-CORDEX suite of simulations has not yet been conducted.

130 Our analysis includes regional-average trends in extreme precipitation as well as local  
131 trends, and we examine both annual-mean and seasonal changes – in winter extreme precipi-  
132 tation over the NEUS is associated with large-scale frontal systems or extratropical cyclones,  
133 whereas in summer extreme precipitation tends to occur in isolated convective systems or in  
134 tropical cyclones. We also investigate the potential drivers of extreme precipitation changes  
135 over the NEUS in terms of thermodynamic and dynamic contributions. While increases  
136 in extreme precipitation are expected due to warmer air’s ability to hold more water vapor,  
137 dynamical changes can modify this picture. Finally, we examine the intermodel spread in  
138 extreme precipitation changes across the NA-CORDEX ensemble members for both the  
139 annual and seasonal analyses. Throughout the analysis, we relate our results to both prior  
140 regional studies of the NEUS as well as to global studies of midlatitude precipitation.

The remainder of the paper is organized as follows. In Section 2, we describe the NA-CORDEX data, the metrics by which we define extreme precipitation, and the techniques used in the analysis. In Section 3 we present the main results and in Section 4 offer further synthesis of the pertinent results, avenues for future research, and conclusions.

## 2. Materials and methods

### *a. Models and simulations*

At the time of writing, the only available version of NA-CORDEX is based on the CMIP5 suite of simulations (Bukovsky and Mearns 2020; McGinnis and Mearns 2021); a revised CORDEX program using CMIP6 is in its early stages of development and the downscaled simulations have not yet been conducted. However, as mentioned in Section 1, Agel and Barlow (2020) found that there was little improvement in the simulation of extreme precipitation over the NEUS in the CMIP6 suite of simulations compared to the CMIP5 suite of simulations (despite the different forcing scenarios of CMIP5 [RCPs] and CMIP6 [SSPs]) and so, assuming the revised CORDEX will use the same RCMs (at the time of writing this has not yet been decided), we expect that our findings will be qualitatively robust in the next generation of experiments.

NA-CORDEX simulations are publicly available at  $0.44^\circ$ ,  $0.22^\circ$ , and  $0.11^\circ$  resolution. We use the  $0.22^\circ$  (25 km) resolution simulations, since the smaller subset of simulations available at  $0.11^\circ$  resolution only cover the historical period. Even if  $0.11^\circ$  simulations were available for future emission scenarios, we expect that they would be largely consistent with the  $0.22^\circ$  simulations, as Lucas-Picher et al. (2016) found that historical  $0.22^\circ$  and  $0.11^\circ$  simulations showed good agreement over the NEUS, and both provided improved agreement with observations compared to  $0.44^\circ$  resolution simulations using a variety of metrics. These improvements were attributed, in part, to better representation of orography.

We use model data that were previously interpolated onto a common grid to provide straightforward comparisons between models (McGinnis and Mearns 2021). While data

167 are available for the entire continental United States, we only consider the NEUS, which  
168 includes Maine, New Hampshire, Vermont, Massachusetts, Rhode Island, Connecticut,  
169 New York, New Jersey, Pennsylvania, Delaware, Maryland, West Virginia, and the District  
170 of Columbia, consistent with the previous studies of Frei et al. (2015); Huang et al. (2017);  
171 Agel et al. (2020); Agel and Barlow (2020) [see Figure 1 for an illustration of this region].  
172 Only surface variables are publicly-available.

173 We use the bias-corrected NA-CORDEX output, which was obtained by the NA-CORDEX  
174 team (McGinnis and Mearns 2021) using the Cannon (2018) multivariate quantile-mapping  
175 algorithm against the gridded, daily Daymet observational data set (which itself is based  
176 on observations from the Global Historical Climatology Network). Such bias-correction is  
177 accepted practice for refining model data to analyze climate change impacts (Kirchmeier-  
178 Young et al. 2017; Zscheischler et al. 2018) and we refer the interested reader to Cannon  
179 (2018) for more information on the bias-correction algorithm and Behnke et al. (2016) for  
180 the uncertainty in Daymet data over regions for which there are few GHCN stations. While  
181 this algorithm minimizes model bias, it does not completely remove all bias, and differences  
182 in model climatologies remain.

183 We use all NA-CORDEX simulations that have publicly-available, daily-averaged,  
184 Daymet-corrected temperature and precipitation data spanning 1950-2100. All calcula-  
185 tions are performed with daily-averaged data, and throughout the analysis we take the  
186 “historical” period to be 1986-2005 and the “projected” period to be 2081-2100. Unless  
187 otherwise stated, we refer to the change in a variable as the difference between its aver-  
188 age value during the projected period and its average value during the historical period.  
189 Simulations of future climate follow the RCP8.5 forcing scenario (i.e. the high emissions  
190 representative concentration pathway (Hausfather and Peters 2020)), which most closely  
191 aligns with recent observations of both CO<sub>2</sub> emissions (Schwalm et al. 2020) and extreme  
192 precipitation (Lopez-Cantu et al. 2020). Furthermore, there are more simulations run us-  
193 ing RCP8.5 than RCP4.5 in the NA-CORDEX ensemble, allowing us to conduct a more  
194 thorough analysis. Since the fractional change in extreme precipitation is not dependent

on the emissions scenario (Pendergrass et al. 2015), we do not expect this choice to have a significant impact on our results.

We have investigated the role of internal variability by considering different historical and projected periods and find that all results presented below are qualitatively robust to the 20 year spans chosen for the historical and projected periods (we also considered the similarly spaced periods of 1950-1969 and 2045-2064, not shown). Hence, while there is certainly internal variability present in the system (Huang et al. 2021), the century-scale extreme precipitation trends calculated here are primarily driven by the prescribed RCP8.5 forcing scenario, consistent with previous modeling studies (Agel et al. 2020; Agel and Barlow 2020).

Global Model	Regional Model	ECS (°C)
CanESM2	CanRCM4	3.7
	CRCM5-UQAM	3.7
GEMatm-Can	CRCM5-UQAM	3.7
GEMatm-MPI	CRCM5-UQAM	3.6
GFDL-ESM2M	RegCM4	2.4
	WRF	2.4
HadGEM2-ES	RegCM4	4.6
	WRF	4.6
MPI-ESM-LR	CRCM5-UQAM	3.6
	RegCM4	3.6
	WRF	3.6
MPI-ESM-MR	CRCM5-UQAM	3.4

Table 1. Global and regional model pairings comprising the 12 available NA-CORDEX simulations with daily, bias-corrected output at 0.22° (~25 km) resolution and forced using RCP 8.5. The equilibrium climate sensitivity (ECS; the temperature change due to a doubling of CO<sub>2</sub>), as diagnosed by Karmalkar (2018) and the NA-CORDEX team (see <https://na-cordex.org/simulation-matrix.html>), is noted for each model.

There are 12 simulations (i.e. unique pairings of GCMs and RCMs) which match the selected spatial/temporal resolutions, bias-correction, and emissions scenario (Table 1). We have disregarded one of the simulations (CanESM2,CanRCM4) in most of our analysis,



213 as this simulation is a clear outlier in the magnitude of the fractional change in extreme  
214 precipitation – the fractional change diagnosed from the CanESM2,CanRCM4 simulations  
215 is double that diagnosed from the average of the other 11 ensemble members (discussed  
216 further in Section 3.3). Additionally, Karmalkar (2018) found that the CanESM2,CanRCM4  
217 simulation was the only NA-CORDEX simulation for which the downscaled precipitation  
218 was greater than the driving model. We have not investigated this pairing further, but note  
219 that it is the only pairing which uses CanRCM4. The ensemble considered here is larger  
220 than those in previous dynamical downscaling studies (Hayhoe et al. 2008; Rawlins et al.  
221 2012), allowing us to better quantify uncertainty.

222 As stated in Section 1, the range of climate sensitivities in the NA-CORDEX ensemble is  
223 advantageous, as earlier studies used models with a much smaller range of sensitivities. For  
224 the 11 ensemble members used here, the equilibrium climate sensitivity ranges from 2.4 to  
225 4.6°C [for reference, the equilibrium climate sensitivity of the full CMIP5 ensemble ranges  
226 from 2.0 to 4.7°C (Andrews et al. 2012; Flato et al. 2014)]. The spread in annual-mean  
227 North American precipitation projections from the downscaled NA-CORDEX simulations  
228 is greater than that of the driving GCMs alone and closer to that of the full CMIP5  
229 ensemble (Bukovsky and Mearns 2020). Regardless of the global or regional model used,  
230 all simulations slightly overestimate the magnitude of average annual precipitation over the  
231 region [1.156 m, based on data from the Global Historical Climatology Network]. Bukovsky  
232 and Mearns (2020) previously showed that the NA-CORDEX overestimates precipitation,  
233 similar to other ensembles (Rawlins et al. 2012), though the dynamical-downscaling of  
234 GCMs with RCMs does minimize the overestimation in precipitation. All 11 simulations  
235 are given equal weighting (i.e. all model projections are considered equally likely) in  
236 calculating the ensemble average for all diagnostic presented in Section 3.

#### 237 *b. Extreme precipitation indices and scaling*

238 Extreme precipitation can be quantified using a number of metrics, including the annual  
239 maximum of daily precipitation (Rx1day), the number of a days in a year with precipitation

exceeding 10mm (R10mm) and the 99th percentile of precipitation (R99) (Schar et al. 2016). After presenting a brief comparison of the metrics in Figure 1, we will generally use R99 to quantify extreme precipitation throughout our analysis to be consistent with previous studies of regional extreme precipitation (Huang et al. 2017; Agel et al. 2018). Also consistent with earlier global modeling studies, we calculate extremes using all days (Ban et al. 2015; O’Gorman 2015), rather than wet days only, since the wet day frequency does not necessarily remain fixed in a warming climate [see Section 2c, and also Schar et al. (2016)].

In presenting spatial data, the metrics are calculated at each grid box for each model, then averaged over the 11 ensemble members to create ensemble-mean maps. For the frequency analysis, daily, regionally-averaged [weighted by area] precipitation is calculated for each model and R99 is taken from this time series. Values of R99 are then averaged across the 11 simulations to derive the ensemble average. Throughout this study, we calculate fractional changes in extreme precipitation [i.e. the percent change in R99 per degree warming], using local, rather than global, warming. While previous studies have calculated this ratio using global-mean warming, we instead use local warming so as to provide regional stakeholders with a more intuitive and localized planning metric. Moreover, we believe that local temperature is more informative for diagnosing the drivers of precipitation changes at the regional scales considered here, although local/regional changes in temperature are often more uncertain than global changes in temperature.

### *c. Power-law distributions*

A convenient method of diagnosing changes in the frequency and intensity of extreme precipitation is to fit power-laws to the probability density functions (PDFs) of daily precipitation. We follow the method of Martinez-Villalobos and Neelin (2019) to do this, in which the PDFs of daily precipitation,  $p$ , are calculated as

$$\text{PDF} = Ap^{-\tau} \exp\left(-\frac{p}{P}\right), \quad (1)$$

where  $A = \Gamma(1 - \tau)^{-1} P^{\tau-1}$ ,  $\Gamma$  is the gamma function,  $\tau$  is the power-law exponent, and  $P$  is the cutoff scale. The value of  $\tau$  represents the probability of light and moderate precipitation days and the value of  $P$  represents the probability of extreme precipitation days. Taking the logarithm of (1) gives

$$\log(\text{PDF}) \sim C_1 + C_2 \log(p) + C_3 p, \quad (2)$$

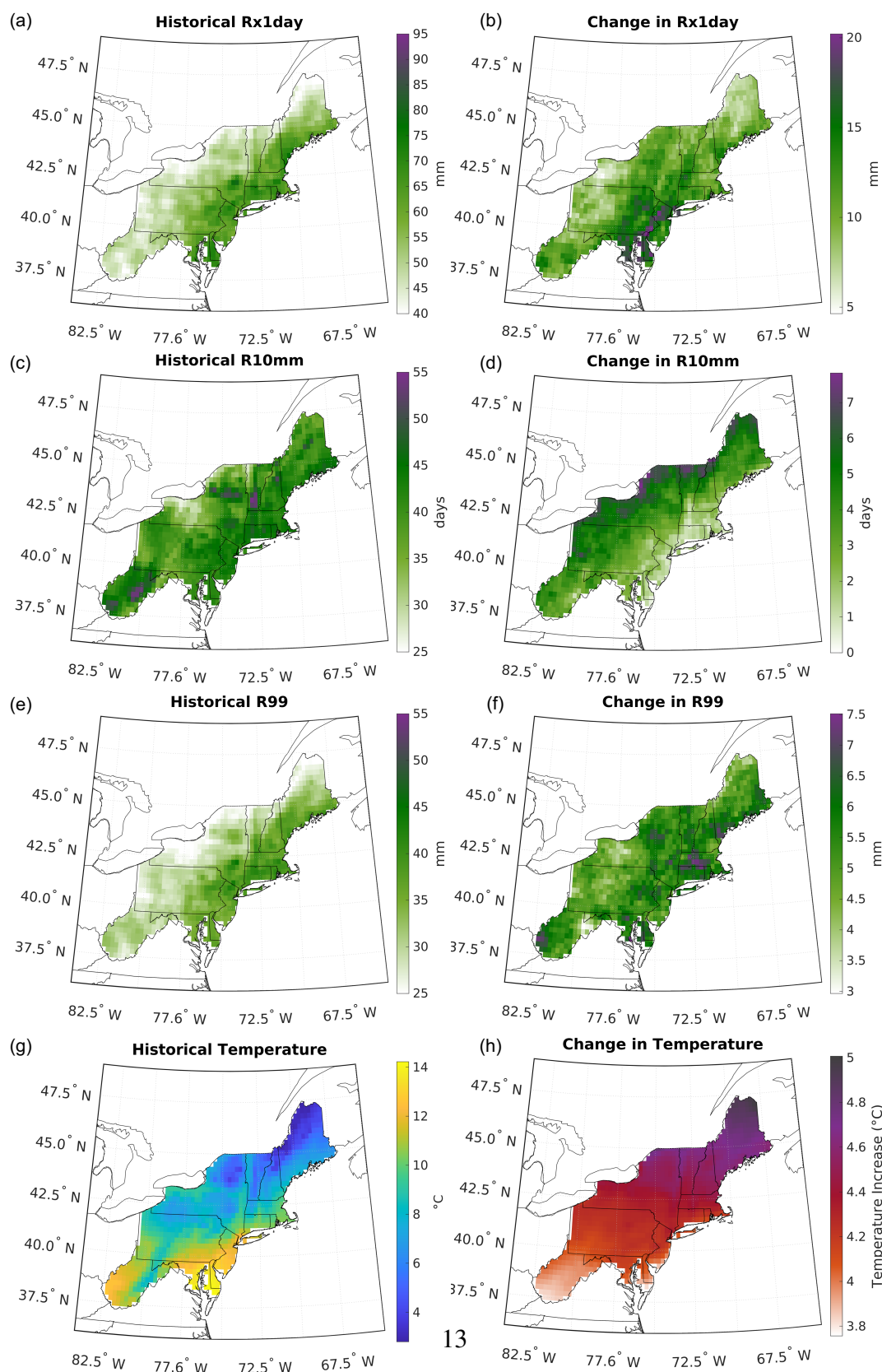
where  $\tau = -C_2$  and  $P = -C_3^{-1}$ . The coefficients  $C_1$ ,  $C_2$ , and  $C_3$  can be obtained by linearly regressing the regionally-averaged, daily precipitation onto the binned probabilities, and then using (2) to obtain  $\tau$  and  $P$ . Once this power law fit has been performed for each simulation, we average the individual simulations' power-law exponents ( $\tau$ ) and cutoff scales ( $P$ ) to derive the ensemble-averaged power-law distribution. This process is completed twice, once for the historical period (giving  $\tau_H$  and  $P_H$ ) and once for the projected period (giving  $\tau_P$  and  $P_P$ ), in order to diagnose regional changes in the frequency of extreme precipitation. A detailed explanation of daily precipitation distributions and a test of this distribution is provided in Martinez-Villalobos and Neelin (2019).

### 3. Results

#### *a. Ensemble-mean, annual-mean changes*

We begin by considering ensemble-mean changes across the NEUS. Averaged over the 11 ensemble-members, the NEUS experiences an annual-mean warming of 3.8-5°C by the end of the 21st century, with the largest warming at higher latitudes (Figure 1h; for reference, the globally-averaged warming across the driving models is 2.4-4.1°C). This latitudinal gradient in warming is consistent with prior studies of the NEUS (Hayhoe et al. 2008; Rawlins et al. 2012) and with the more general Arctic amplification of warming seen throughout the Northern Hemisphere in climate projections [e.g. Pithan and Mauritsen (2014)].

Changes in extreme precipitation do not exhibit such a clear latitudinal gradient. Instead, the changes in both Rx1day and R99 are largest in coastal regions and smaller further



13

Figure 1. Historical (left panels) and change (right panels) in extreme precipitation (as quantified by Rx1day [a-b], R10mm [c-d], and R99 [e-f]) and temperature (g-h). There is relatively good agreement in the historical a) Rx1day and e) R99 metrics, with extreme precipitation having a coastal dependence, as is also the case in panels (b) and (f) showing the change in indices.

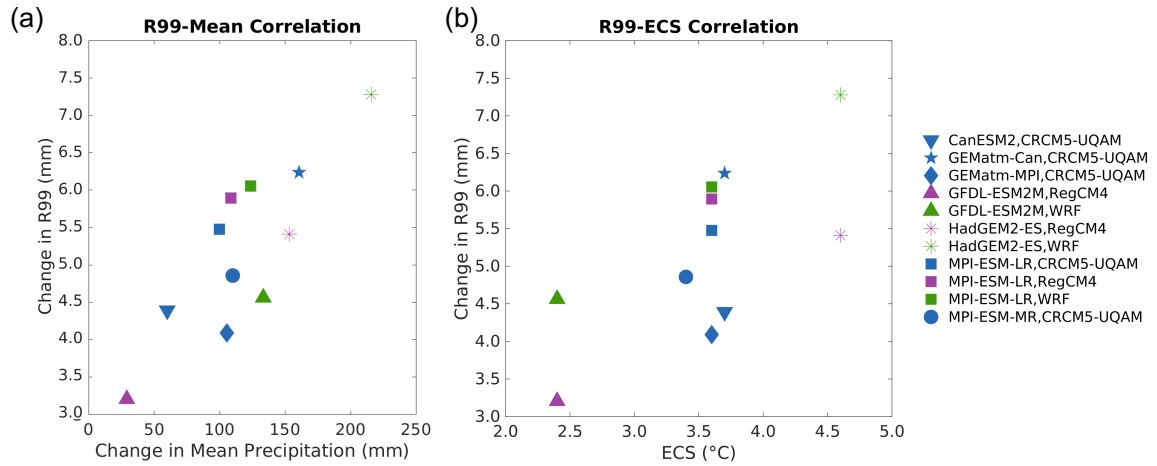


Figure 2. a) Correlation between the change in mean precipitation and the change in extreme precipitation (R99). b) Correlation between the simulations' equilibrium climate sensitivity (ECS) and change in NEUS-average extreme precipitation (R99).

inland (Figure 1b,f). Eastern Pennsylvania and New Jersey are projected to experience increases in Rx1day of up to 20mm/day, while southern Massachusetts is projected to see increases in R99 of 7.5mm/day. These patterns reflect the simulated and observed historical patterns of Rx1day and R99, which are also largest in coastal regions (panels a and e), consistent with Huang et al. (2017). For c), d) R10mm, however, there is less of a coastal dependence, and a stronger coupling with orography, with peaks in extreme precipitation over mountain regions, such as the Appalachian, Adirondack, Green, and White Mountains. For Rx1day and R99, the presence of orographically-driven precipitation is less pronounced. The relative agreement in the sign and spatial pattern of changes in Rx1day and R99 over the NEUS shown here is consistent with the analysis of Sillmann et al. (2013), who noted that the NEUS is one of the few regions where there is agreement among these indices in diagnosing trends in extreme precipitation.

Averaged over the region, R99 increases by approximately 5.7 mm (with a standard deviation of 0.3 mm), and the change is correlated across the ensemble with the change in

mean precipitation (see Figure 2a), as has been seen in projections of extreme precipitation in downscaled simulations of other regions (Nishant and Sherwood 2021). This change in R99 corresponds to an increase of approximately 20% between the historical and projected periods (separated by 95 years), which yields an increase in extreme precipitation of ~2%/decade, consistent with the historical rate of increase (Hoerling et al. 2016). That the rate of change is robust regardless of the time period considered suggests that the long-term anthropogenically-induced warming is more important than climate variability in establishing extreme precipitation trends over the region on multi-decadal time-scales, which is consistent with the results of Pendergrass et al. (2015).

R10mm exhibits the opposite spatial pattern to the other two metrics, with the smallest increases in coastal regions and the largest increases furthest inland (Figure 1d). To explain this pattern, Figure 3a shows a power-law fit to the regionally-averaged daily precipitation over the historical and projected time-periods. Increases are seen in the occurrence of days with very low precipitation (<1mm) and in the days with extreme precipitation days (>10mm), while the number of days with moderate precipitation is projected to decrease. Note that Wang et al. (2020) found disagreement in the change in extreme precipitation frequency in their statistically-downscaled ensembles, but the NA-CORDEX simulations show good agreement in the change in frequency.

Increases in the frequency of high precipitation days are seen at individual locations as well, and so, since 10mm/day is a moderate rate of precipitation in coastal regions (Figure 3b) and a more extreme rate inland (Figure 3c), the largest changes in R10mm are seen in inland regions. The increase in occurrence of days with extreme precipitation is particularly notable in Figure 3a, as the frequency of the strongest events increases by as much as a factor five compared to the historical simulations. The 90% confidence intervals further underscore the robustness of these increases.

As a different way of showing the increase in the number of strong precipitation events, Figure 4 plots the ensemble-averaged increase in frequency at different percentiles of the control climate. This can also be thought of as the increase in frequency of a particular

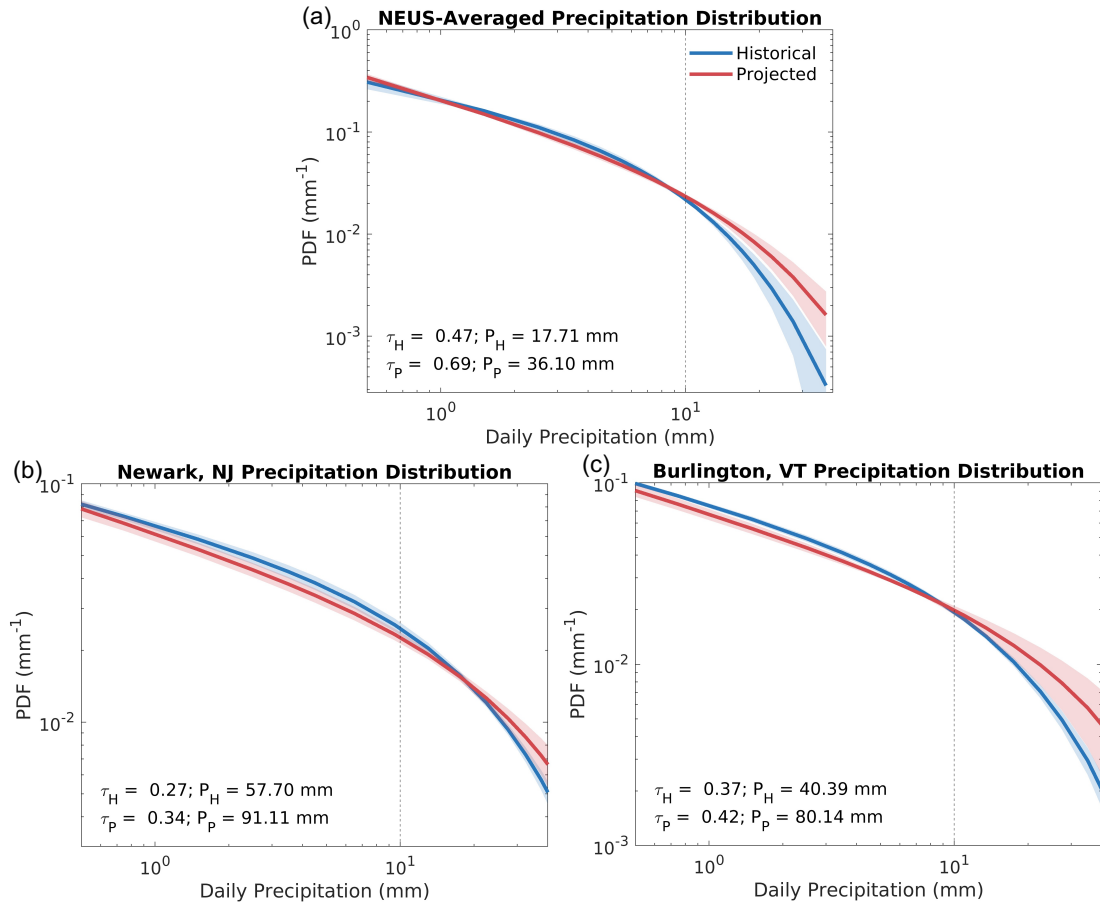


Figure 3. Ensemble-averaged power law distribution of daily precipitation from the 20-year historical (blue) and projected (red) periods for a) the entire NEUS, b) Newark, NJ [40.74N, 74.17W], a typical coastal location, and c) Burlington, VT [44.48N, 73.21W], a typical inland location. Shading indicates the 90% confidence interval. Note that the scales of the vertical axes vary in each panel.

return time compared to the control climate (i.e., a 1-in-10 year event in the control climate becomes approximately 80% more likely by the end of the 21st century for each degree of warming). Given a temperature increase of approximately 5°C (Figure 1h), Figure 4 indicates a factor of five increase in the frequency of the strongest storms, consistent with Figure 3a [this result is likewise consistent with Allen and Ingram (2002), Walsh et al. (2014), and Myhre et al. (2019), among others].

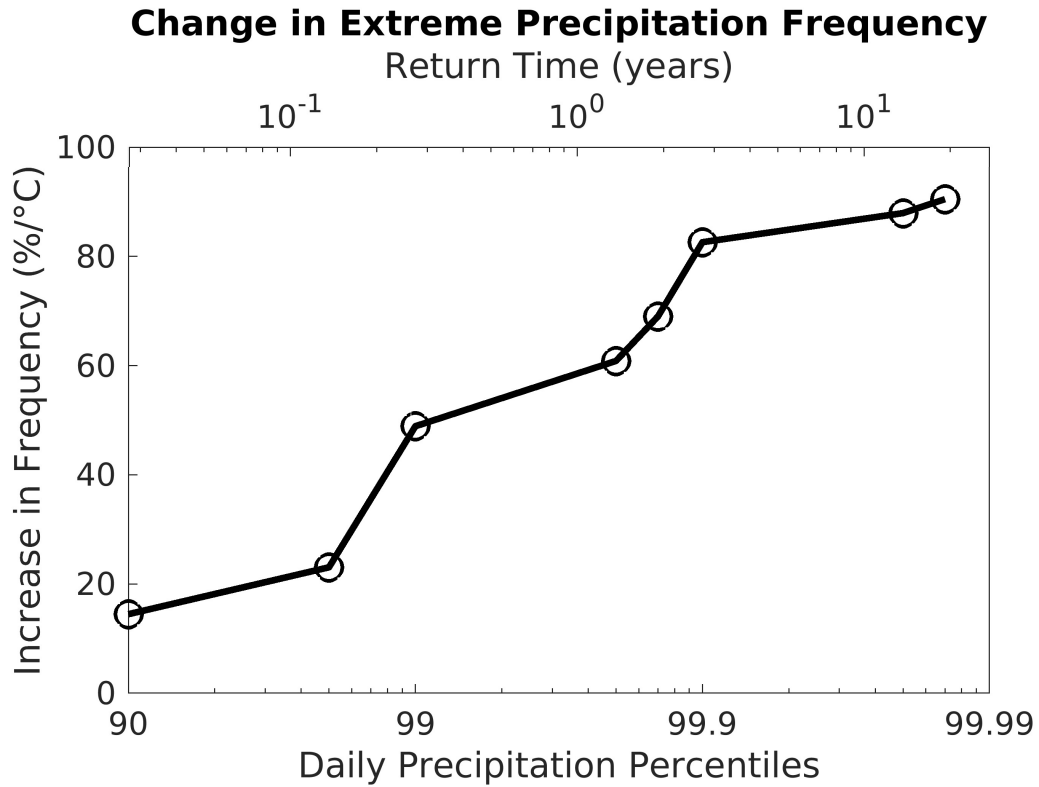


Figure 4. Ensemble-averaged change in storm frequency (as measured through various percentiles) per degree of local warming. Corresponding return times are noted; for example the change in the frequency of the (historical) 99.9 percentile storm is equivalent to the change in frequency of the ~1-in-3 year storm. While not shown here, there is larger intermodel spread for higher percentiles, given the increasingly small sample size.

#### *b. Seasonal changes*

We now discuss changes in extreme precipitation over the seasonal cycle, focusing on the R99 metric. The pattern of extreme precipitation changes is generally similar throughout the year (Figure 5, right panels), with the exception of summer (June-July-August, JJA), when the increases in R99 are smaller and exhibit an inland bias rather than a coastal bias.



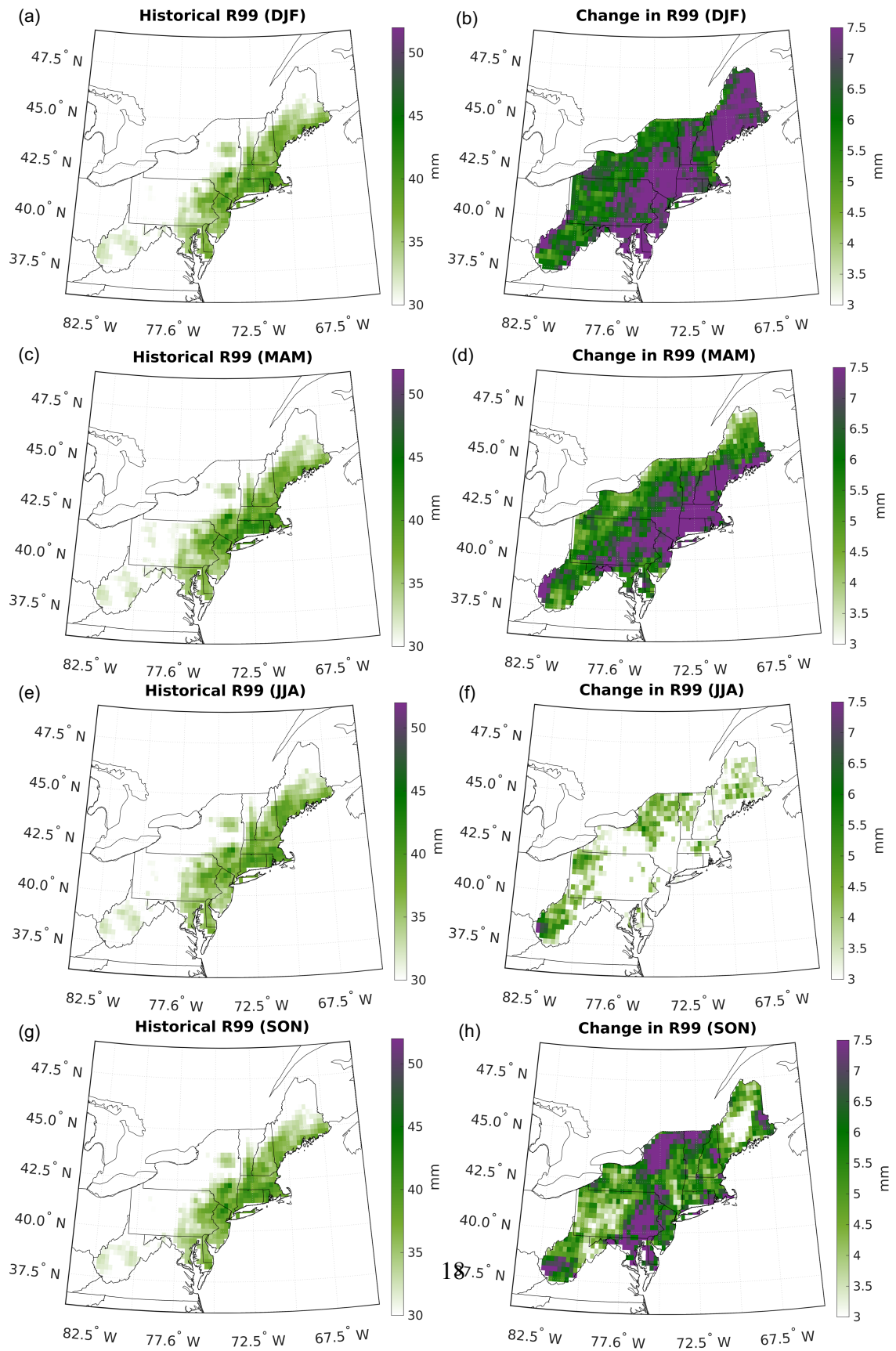


Figure 5. As in Figure 1e,f, but now considering the a,b) winter, c,d) spring, e,f) summer, and g,h) fall historical (left panels) and change in (right panels) extreme precipitation (R99).

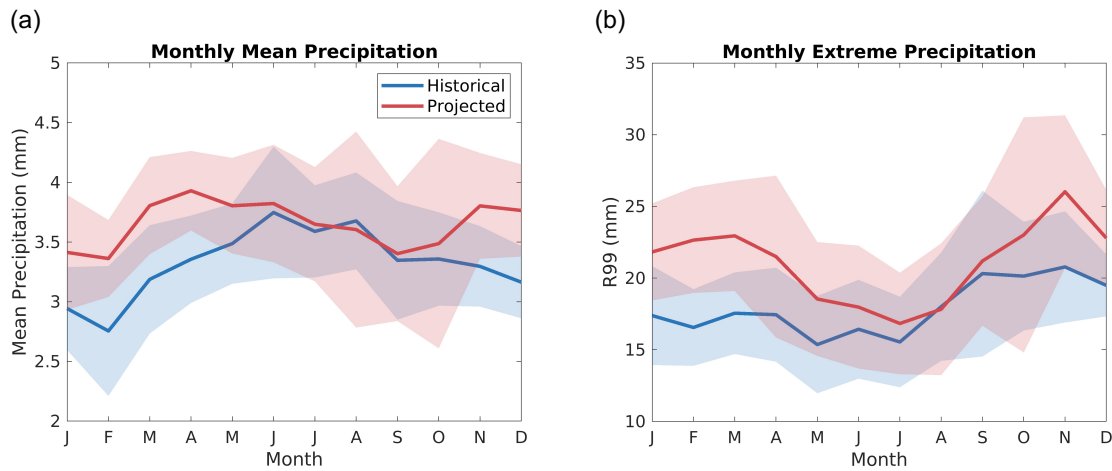


Figure 6. Average monthly mean precipitation (a) and average monthly extreme precipitation (b), measured using R99, over the (blue) historical and (red) projected periods. Shading indicate the 90% confidence intervals.

In the historical simulations the magnitude and pattern of extreme precipitation in JJA is comparable to other seasons (see Figure 5), and we have been unable to identify what causes the difference in the summer response compared to the other seasons. We note that there is significant intermodel spread during summer [see Section 3d], which suggests that models struggle to capture the changes in convective precipitation, which is common over the NEUS during the summer (see Section 4 for further discussion).

The largest increase in extreme precipitation is seen in winter (December-January-February, DJF), when a large swath of coastal NEUS sees increases of up to 8 mm/day in R99. Similarly large increases are seen in spring (MAM) and, for only some inland regions, fall (SON). We speculate that the processes which lead to enhanced wintertime precipitation, such as extratropical cyclones and frontal systems, which is clearly enhanced (panel b), may also be occurring more during the shoulder seasons (spring and fall), but further study is required. Given the spatial pattern of fall extreme precipitation trends (panel h), we do not expect that increases in tropical cyclone-driven extreme precipitation is driving this increase (this is discussed further in Section 4).

Figure 6 shows the seasonal cycles of mean and extreme precipitation averaged over the NEUS region. Consistent with Figure 5, the largest increases in both metrics are seen in winter/spring (November to May) and the smallest increases are seen in summer/early fall (June-September). However, the ensemble-spread in both monthly mean and extreme precipitation is large, and the changes are not statistically significant when averaged over the region. Despite the intermodel spread, Figure 6 is reasonably consistent with seasonality results from earlier studies of regional trends (Hayhoe et al. 2008; Rawlins et al. 2012).

### c. Drivers of changes in extreme precipitation

Extreme precipitation is generated by strong updrafts, such that the rate of extreme precipitation ( $P_e$ ) can be approximated as:

$$P_e \approx \int -\rho w \left( \frac{dq_s}{dz} \right) dz, \quad (3)$$

where  $\rho$  is the air density,  $w$  is the vertical velocity,  $q_s$  is the saturation specific humidity, and  $z$  is the vertical coordinate. We ignore changes in precipitation efficiency, which measures the efficiency with which cloud condensation is converted into precipitation. Precipitation efficiency, particularly of extreme precipitation, is an active area of research [see, for instance, Singh and O’Gorman (2014); Langhans et al. (2015); Lutsko and Cronin (2018); Abbott et al. (2020)], and it is difficult to compare across models with different microphysics schemes, particularly given the available data for NA-CORDEX. However we caution that what we infer to be dynamical changes may actually reflect undiagnosed changes in cloud microphysics.

This expression can be used to decompose fractional changes in  $P_e$  as:

$$\frac{\delta P_e}{P_e} = \underbrace{\left( \frac{\int \rho w \delta \left( \frac{dq_s}{dz} \right) dz}{\int \rho w \left( \frac{dq_s}{dz} \right) dz} \right)}_{\text{thermodynamic}} + \underbrace{\left( \frac{\int \delta(\rho w) \left( \frac{dq_s}{dz} \right) dz}{\int \rho w \left( \frac{dq_s}{dz} \right) dz} \right)}_{\text{dynamic}} + \underbrace{\left( \frac{\int \delta(\rho w \left( \frac{dq_s}{dz} \right)) dz}{\int \rho w \left( \frac{dq_s}{dz} \right) dz} \right)}_{\text{nonlinear}} \quad (4)$$

where  $\delta$  is the difference between the projected and historical periods. The first term is the thermodynamic contribution to the change in extreme precipitation which, from the Clausius-Clapeyron relation, is approximately  $+6\text{-}7\%/^{\circ}\text{C}$ . The second term is the contribution from dynamical changes, and is typically  $\pm 2\%/^{\circ}\text{C}$ . The final term is the contribution from nonlinear changes, and is typically an order of magnitude smaller than the other two terms. As mentioned in Section 2.2, all fractional changes will be taken with respect to local, rather than global, temperature change. We cannot explicitly calculate the individual terms in (4) since only surface-level data is publicly-available and individual modeling centers were only able to provide data at a few vertical levels, which is insufficient to calculate the vertical integrals.

Most of the NEUS experiences fractional increases in extreme precipitation of  $2\text{-}5\%/^{\circ}\text{C}$ , with a regional average increase of  $3.6\%/^{\circ}\text{C}$  (Figure 7a). This is consistent with previous global modeling studies showing that increases in extreme precipitation generally fall below the Clausius-Clapeyron value of  $6\text{-}7\%/^{\circ}\text{C}$  in the extratropics (Kharin et al. 2013; O’Gorman 2015). Additionally, the Clausius-Clapeyron rate is less than  $7\%/^{\circ}\text{C}$  when using local warming rather than global warming, but still larger than the fractional increases seen here.

The smaller fractional increases in the NEUS suggest that dynamical changes – decreases in the speed of updrafts associated with extreme precipitation events – damp the changes in extreme precipitation. Given the lack of publicly-available data at different atmospheric levels, we have not been able to investigate these changes further, but note that a decrease in the dynamical contribution is at odds with a recent model study which showed that storm updrafts will increase (particularly for the strongest storms) in a warming climate (Tamarin-Brodsky and Hadas 2019). The importance of circulation changes in driving changes to vertical velocity was previously shown in the idealized simulations of Pendergrass et al. (2016) and Pendergrass and Gerber (2016).

Interestingly, the fractional changes in R99 exhibit a strong latitudinal dependence, with the smallest fractional changes in the northeastern part of the region (Maine, eastern New Hampshire, eastern Massachusetts) and the largest fractional changes in the southwestern

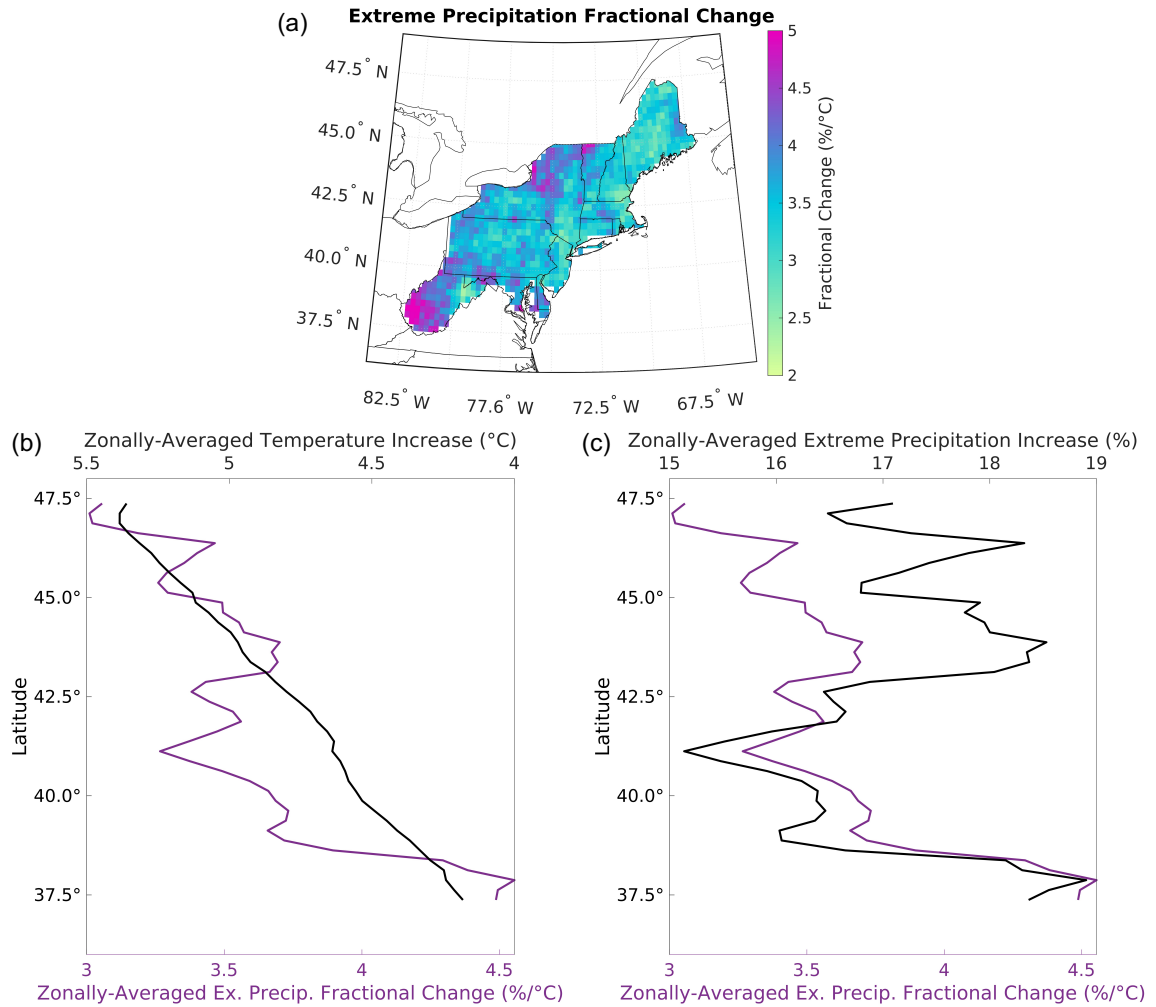


Figure 7. a) Fractional changes in ensemble-average extreme precipitation. The zonally-averaged change in temperature (b, black line) and percent change in R99 (c, black line) are plotted as a function of latitude, with the fractional change superimposed (b and c, purple line). Note the different scales for the secondary horizontal axes.

portion of the region (southwest Pennsylvania and West Virginia) as well as upstate New York (Figure 7b,c; note that this pattern is also qualitatively consistent across seasons – see Figure 8). This is the opposite of the temperature response, and leads to a relatively latitudinally-homogeneous change in extreme precipitation (Figure 1f). Changes in extreme

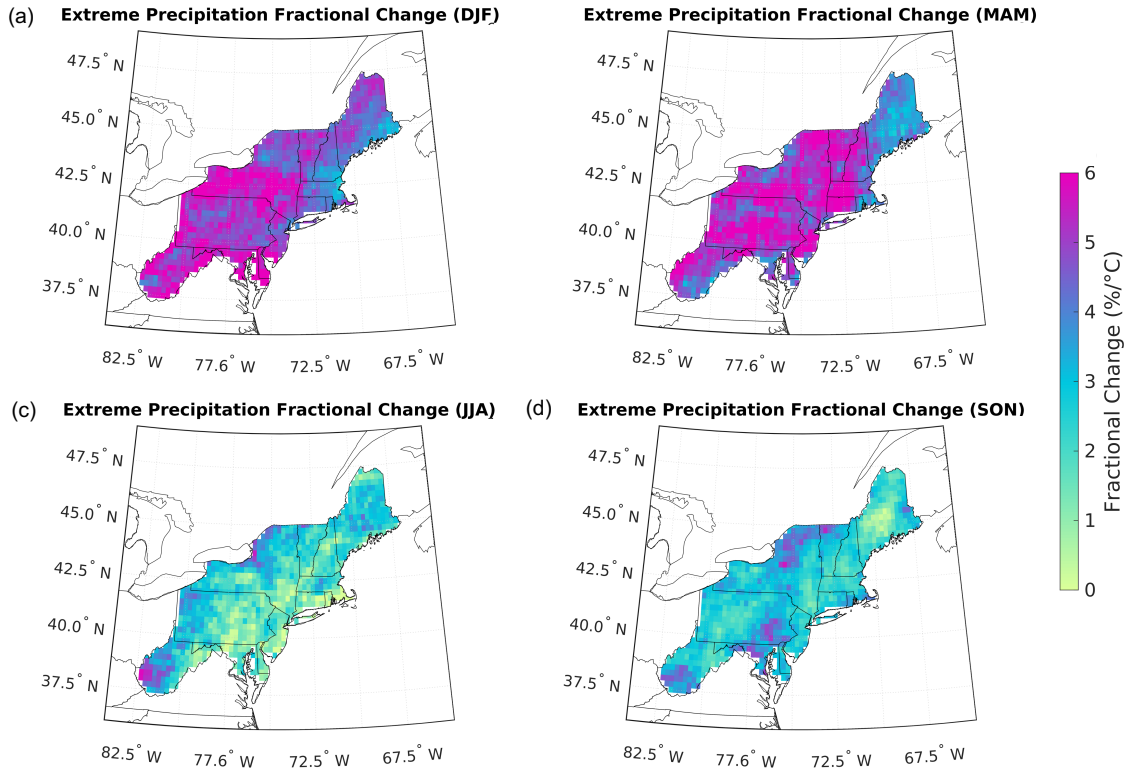


Figure 8. As in Figure 7a, but for a) winter, b) spring, c) summer, and d) fall.

precipitation depend on the changes in temperature associated with individual storms, rather than changes in mean temperature. The former may be more spatially-homogeneous than the latter, which would produce a more spatially-homogeneous distribution of  $\delta P_e$ . We return to this point in the discussion of Section 4.

#### *d. Intermodel spread*

The intermodel spread in the response of regionally-averaged annual-mean R99 is linked to the models' climate sensitivities: more sensitive models produce larger increases in R99 over the NEUS (Figure 2b). However, the NA-CORDEX ensemble members show good agreement in the magnitude of the fractional change in R99, with an ensemble-mean value

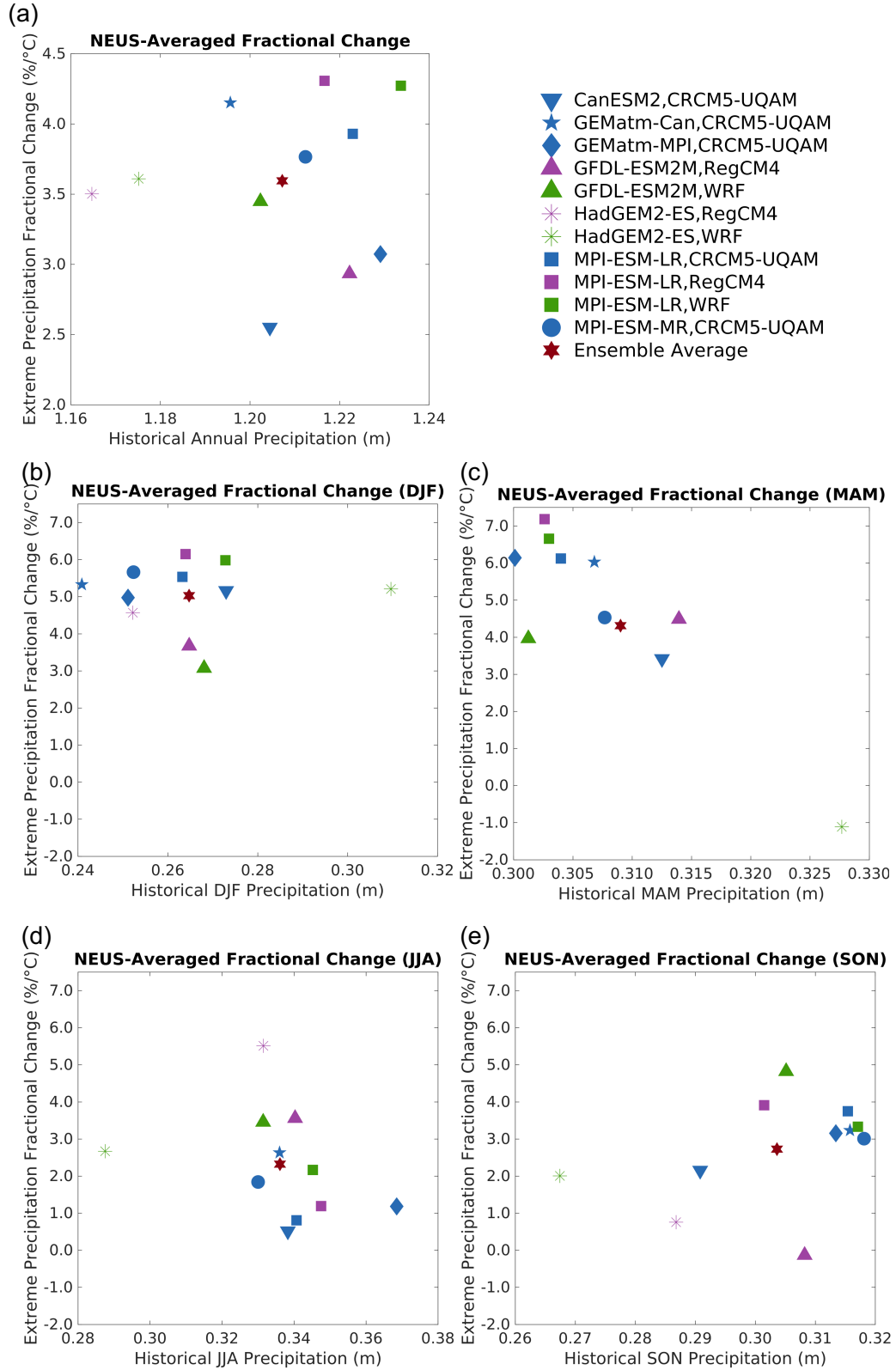


Figure 9. The regionally-averaged a) annual, b) winter, c) spring, d) summer, and e) fall extreme precipitation fractional change for each of the 11 models considered in this study. Individual NA-CORDEX simulations (as well as the ensemble average) are labelled, with each global (i.e. driving) model having a unique marker and each regional model having a unique color. Note the different vertical scale for the annual (a) and seasonal (b-e) fractional changes.

of  $3.6 \pm 0.2\%/^{\circ}\text{C}$  (Figure 9a). Other metrics of extreme precipitation, such as R99.5, Rx1day, and R10mm, give similar fractional changes (not shown).

The lack of significant spread in the fractional change of extreme precipitation is noteworthy for two reasons. First, the driving models have a large spread in both climate sensitivity and in mean precipitation over the historical period. The latter reflects differences in the representation of precipitation-formation processes, which could also drive differences in the response of precipitation. However, the lack of correlation between mean precipitation and the fractional change in extreme precipitation (Figure 9a) suggests that the changes over the NEUS are robust across the physical processes resolved in these downscaled simulations. Second, several previous studies have shown that global models give inconsistent (in magnitude and, in some locations, sign) extreme precipitation trends over different regions (Sillmann et al. 2013), yet all of the model pairings considered here give positive extreme precipitation trends, with a small spread in magnitude. Both of these reasons give confidence in our estimate of the fractional change of  $3.6 \pm 0.2\%/^{\circ}\text{C}$  over the NEUS.

For the same GCM, the spread in extreme precipitation fractional change across the different regional model pairings is small, which suggests that the driving model is primarily responsible for the extreme precipitation trend (see, for instance, the HadGEM2 ensemble members in Figure 9a).

We consider the fractional change in extreme precipitation as a function of season and GCM-RCM pairing in Figure 9b,c,d,e (see Figure 8 for the corresponding plots of ensemble-averaged fractional change in extreme precipitation and Figure 10b-e for the standard error in seasonal extreme precipitation). The model-averaged fractional changes for winter, spring, summer, and fall are  $5.0\%/^{\circ}\text{C}$ ,  $4.7\%/^{\circ}\text{C}$ ,  $2.3\%/^{\circ}\text{C}$ , and  $2.7\%/^{\circ}\text{C}$ , respectively (if the change in temperature is small for a grid box, the regionally-averaged change in temperature is used instead, so as to avoid unrealistically large fractional changes; this occurs in less than 5% of the grid boxes over all simulations). Figure 9 illustrates that, for all seasons, there is significantly more spread in the seasonal fractional change (and in R99, Figure 10b-e) than in the annual-mean fractional change, with a couple models yielding negative



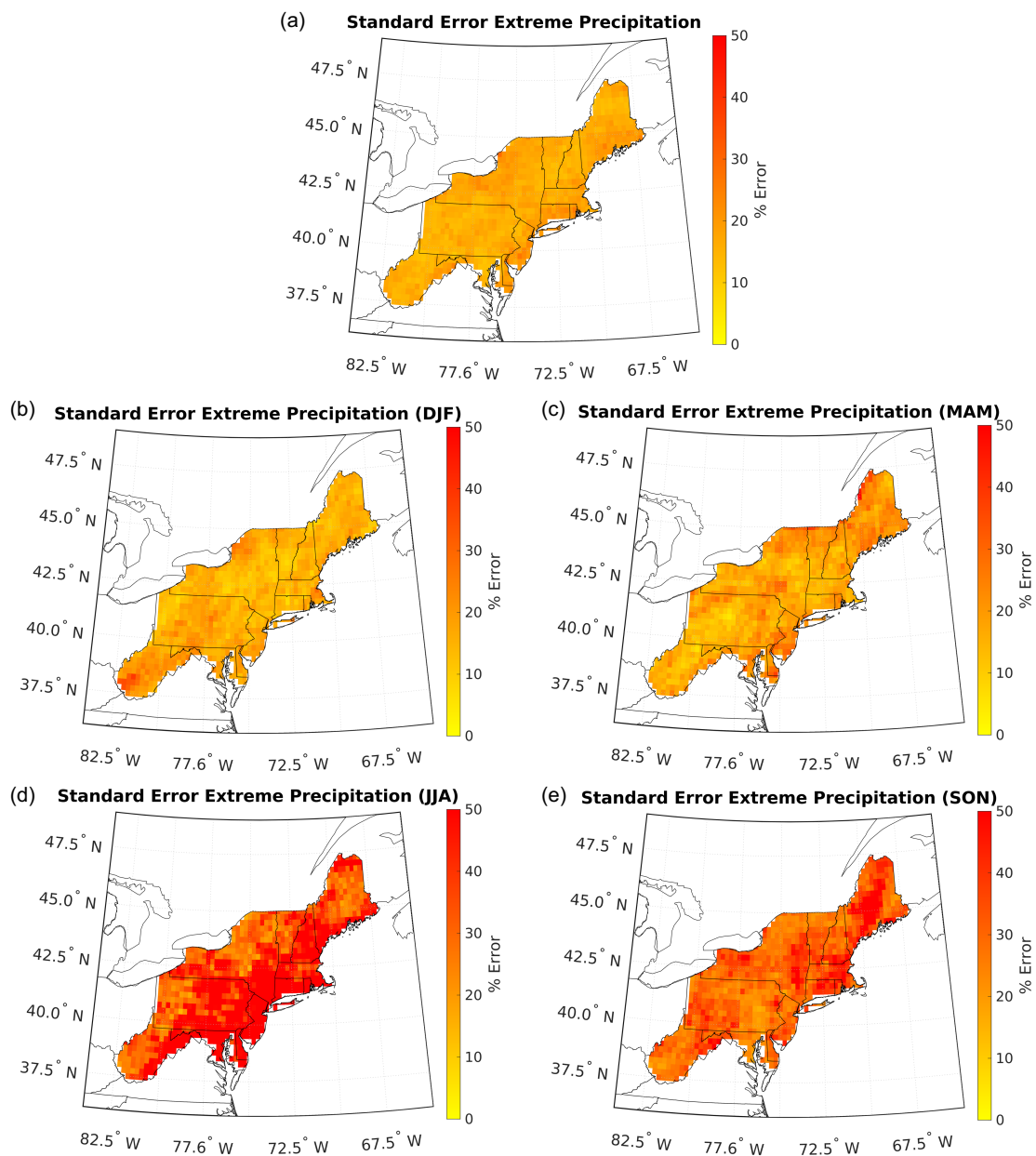


Figure 10. The a) annual, b) winter, c) spring, d) summer, and e) fall percent error in the change in R99 over the 11 ensemble members. To calculate the percent change, the standard error in R99 across the ensemble is normalized by the ensemble average change in R99 and multiplied by 100 at each grid box.

fractional changes due to projected cooling during the shoulder seasons (MAM and SON). The HadGEM2-ES,RegCM4 simulation is not shown for spring (panel c) since the fractional change is a large negative value due to unrealistic cooling.

While the annual extreme precipitation fractional change over the NEUS does not depend on the simulation's historical mean precipitation (Figure 9a), Figure 9d,e shows that the summer and fall extreme precipitation fractional change may be inversely related to the historical mean precipitation: for summer and, to a greater extent, fall, simulations with lower historical seasonal precipitation experience a larger increase in extreme precipitation. All of the NA-CORDEX simulations overestimate mean annual and seasonal precipitation compared to that of the Global Historical Climatology Network (although, not as much as the CMIP5 ensemble), which implies that the actual extreme precipitation fractional change may be larger than the means presented here given this inverse relationship. This would suggest that, while the absolute value of extreme precipitation increases the most during the winter and spring months (see Figure 6), the fractional change in extreme precipitation is larger during the summer and fall, and closer in magnitude to the Clausius-Clapeyron scaling. This is consistent with recent downscaled simulations of Massachusetts which show the largest extreme precipitation fractional change occurring during the summer (Steinschneider and Najibi 2022).

Finally, in terms of the pattern of the extreme precipitation response, most ensemble members exhibit a coastal intensification of extreme precipitation (Figure 11), though there are several members which show more homogeneous patterns of R99 change (i.e., GEMatm-Can,CRCM5-UQAM and HadGEM2-ES,WRF). The standard error is roughly constant over the region (Figure 10a) and is generally small compared to the change in extreme precipitation (approximately 15%). There are no parts of the NEUS in which the response of extreme precipitation seems to be especially uncertain. The intermodel spread in the change and fractional change in extreme precipitation is small during winter and spring (Figures 9b,c and 10b,c) and significantly larger during summer and fall (Figures 9d,e and 10d,e), suggesting that the processes responsible for the changes in extreme precipitation

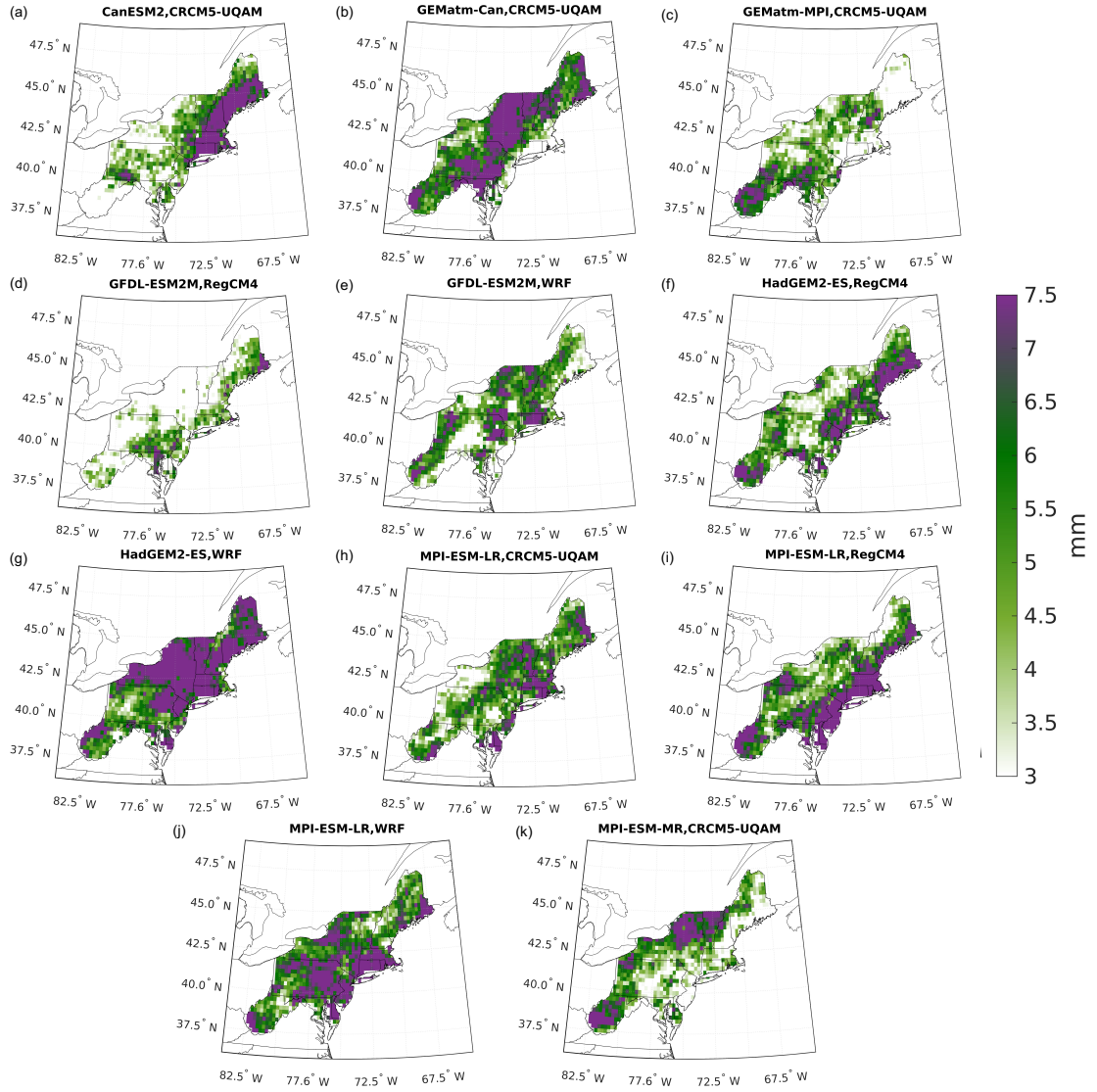


Figure 11. Spatial distribution of the change in extreme precipitation (R99) for the 11 ensemble members considered in this study.

for these seasons (i.e. isolated convective systems and tropical cyclones) is poorly captured across the models.

The majority of the ensemble members likewise agree on the spatial pattern of the fractional change in annual precipitation (Figure 12), with the largest values ( $\sim 6\%/^{\circ}\text{C}$ ) in

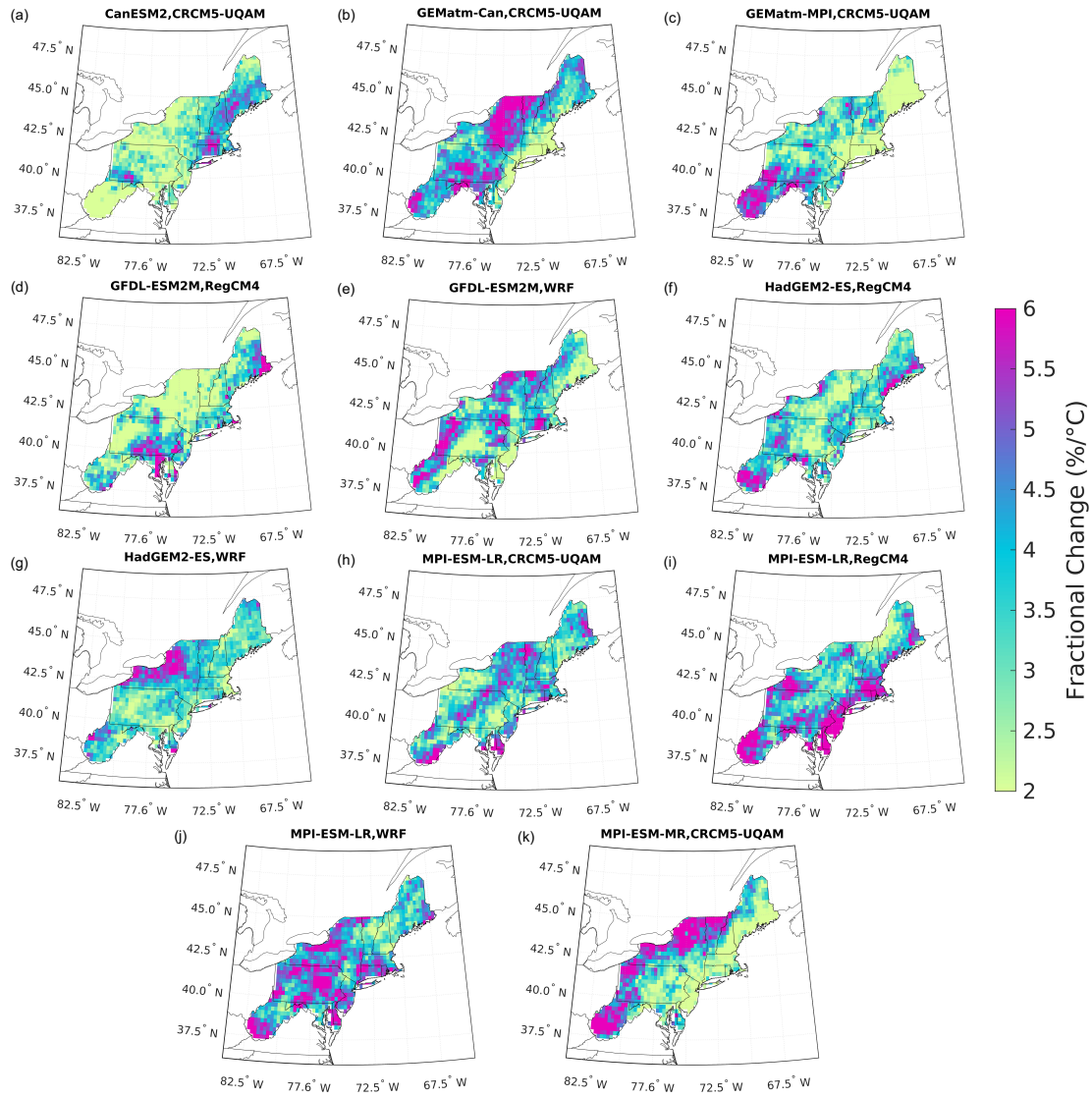


Figure 12. Spatial distribution of the fractional change in extreme precipitation for the 11 ensemble members considered in this study.

the southwest portion of the region and upstate New York and the smallest values ( $\sim 2\%/^\circ\text{C}$ ) in the northeast portion of the region (the CanESM2 ensemble member (panel a), however, is not consistent with the spatial pattern of other 10 members).

## 4. Discussion and Conclusions

In this study, we have used the NA-CORDEX ensemble to make the first comprehensive assessment of changes in extreme precipitation over the NEUS using a large suite of dynamically-downscaled simulations encompassing a broad range of climate sensitivities. The use of high-resolution, dynamically-downscaled simulations is essential for obtaining accurate and robust projections of future extreme precipitation at the scales required for planning and adaptation purposes.

Averaged over the region, we find that in the ensemble-mean the 99th percentile of daily precipitation (R99) increases by  $5.7 \pm 0.3$  mm by the end of the 21st century under the RCP8.5 scenario, an increase of approximately 20% compared to the end of the 20th century, or a rate of  $3.6\%/^{\circ}\text{C}$  of warming. This is consistent with the historical rate of increase of roughly 2%/decade (Hoerling et al. 2016). Examining PDFs of regionally-averaged, daily-mean precipitation shows a general tendency for increases in the number of dry days and in days with heavy precipitation over the course of the 21st century, with relatively fewer days of moderate precipitation ( $\sim 1$ -10 mm). While this is consistent with projections of precipitation in other mid-latitude regions, which show a similar pattern of rainfall becoming more intermittent but more intense, this was not seen in the earlier, high-resolution simulations of the NEUS of Wang et al. (2020) and represents an advancement of our understanding of changes in extreme precipitation frequency. Compared to the end of the 20th century, extreme precipitation events over the NEUS may become up to five times more frequent in the last decade of the 21st century.

The changes over the NEUS show a marked coastal bias, with the largest increases in coastal regions [consistent with Thibeault and Seth (2014)] and smaller increases occur further inland. For instance, southern Massachusetts (coastal) is projected to see an increase in R99 of up to 7.5 mm/day, while parts of upstate New York (inland) may see increases of just 3 mm/day. This coastal bias reflects the historical pattern of extreme precipitation.

The increases in R99 are not evenly distributed throughout the year; the smallest changes are generally seen in summer and, to a lesser extent, fall (see Figures 5f, 6b, and 9d). This result contrasts with earlier observational studies which have shown the largest increases in extreme precipitation during the warm season (Frei et al. 2015) (note, however, that the seasonal changes are less robust, particularly when averaging over the entire region [see Figure 6b and 10b]). This result, coupled with the atypical inland spatial pattern of extreme precipitation change over summer (Figure 5f) and the small increase in extreme precipitation over the start of the fall (Figure 6) suggests that the NA-CORDEX ensemble may not fully capture the extreme precipitation associated with tropical cyclones over the NEUS, which are expected to lead to more coastal extreme precipitation (Garner et al. 2021). Rendfrey et al. (2021) used three WRF simulations from the NA-CORDEX ensemble (at  $0.22^\circ$ ) and found that coastal portions of the region will experience an increase in tropical cyclone-associated annual precipitation of 20 mm/year, although the results were not robust across the NEUS and this is less than a third of the ensemble size considered in this study. The role of tropical cyclones and, in particular, the seasonality of extreme precipitation associated with tropical cyclones in NA-CORDEX warrants further study. Additionally, it is well-documented that models (even at  $0.22^\circ$  resolution) poorly resolve convection, which is the primary driver of JJA extreme precipitation over the NEUS. Given the limited ability of models to capture convectively-driven extreme precipitation, it is not surprising that simulations do not necessarily capture the change in summertime extreme precipitation seen in observations (Frei et al. 2015).

One of the benefits of conducting dynamical downscaling studies is the more realistic representation of precipitation due to surface forcing, such as orography. NA-CORDEX reasonably resolves historical orographic precipitation, particularly on the climatological windward side of mountains (see Figure 1c), but, regardless of the metric, Figure 1b,d,e does not show notable changes in extreme precipitation in regions of significant orography (such as the Appalachian, Adirondack, Green, or White Mountains). Prior work suggests that the climatological leeward sides of mountains will experience increases in extreme

574 precipitation in a warming climate (O’Gorman (2015) and references therein), but that is  
575 not seen in this ensemble of dynamically-downscaled simulations and provides an avenue  
576 for further research as well as a potential metric for evaluating downscaled simulations.

577 Furthermore, we have not considered the impacts of urbanization in this study or other  
578 dynamic land changes and associated feedbacks on extreme precipitation. Such analysis  
579 with CORDEX has been conducted for Africa (Soares et al. 2019), Europe (Knist and  
580 coauthors 2017), and Middle East and Northern Africa (Constantinidou et al. 2020) and  
581 was the primary focus of these studies. While we have not conducted a sweep of land  
582 surface schemes here, we expect that, based on the work of Singh et al. (2020), urbanization  
583 would exacerbate the increase in extreme precipitation over much of the NEUS. Much of  
584 this region, particularly the coastal communities, are densely populated which Singh et al.  
585 (2020) showed has an amplifying effect on extreme precipitation trends. If we continue  
586 to follow this high emissions scenario and the region continues to become more densely  
587 populated, the increases in extreme precipitation presented here for the NEUS may represent  
588 lower bounds on the actual increases.

589 Over most of the NEUS, extreme precipitation increases by 2-5% per degree C of local  
590 warming, which is less than would be expected from thermodynamic considerations alone  
591 and suggests that dynamical changes are damping the increase in extreme precipitation (as  
592 noted in Section 2.2, this difference is also due, in part, to considering the local rate, and not  
593 the global rate, of warming). Furthermore, this fractional change in extreme precipitation is  
594 seasonally-dependent, with all seasons experiencing a sub-Clausius Clapeyron increase; the  
595 largest change occurring in winter time (approximately  $+5\%/^{\circ}\text{C}$ ) and the smallest change in  
596 summer (approximately  $+2\%/^{\circ}\text{C}$ ). Based on the publicly-available output for NA-CORDEX,  
597 we cannot diagnose the causes of these dynamic changes, but a slowdown of updraft speeds  
598 associated with extreme precipitation events is implied in contrast to the recent study of  
599 Tamarin-Brodsky and Hadas (2019). This is a novel result and warrants further study. It  
600 is also worth noting that the temperature response exhibits a latitudinal gradient, such that  
601 higher latitudes warm more, but the changes in extreme precipitation do not show such

a gradient. This means that the fractional changes in extreme precipitation are largest in the southern portion of the NEUS and smallest in the north. We interpret this as changes in extreme precipitation depending more on the temperatures associated with individual extreme events, rather than on changes in average temperatures, with the former more evenly distributed in latitude than the latter. However, at present it is unclear which temperatures to use when diagnosing the drivers of changes in extreme precipitation at the regional scale. Global- or regional-mean temperatures may not provide the entire story and detailed tracking of the storms which produce extreme precipitation in the NEUS will likely be needed to fully understand what drives the changes in extreme precipitation described here.

The ensemble members participating in NA-CORDEX generally show good agreement in the regionally-averaged change in extreme precipitation, and most of the spread in the magnitude of the R99 response averaged over the region comes from ensemble members' equilibrium climate sensitivities. The ensemble members also generally agree on the qualitative pattern of the extreme precipitation response (i.e., the coastal amplification). One exception is CanESM2,CanRCM4, which projects much larger increases in extreme precipitation than the other ensemble members, roughly following the scaling implied by the Clausius-Clapeyron relation. CanESM2,CanRCM4 is the only NA-CORDEX simulation for which the downscaled precipitation is greater than the driving model, and is also the only pairing which uses CanRCM4. Given the good agreement between the other model pairings, we believe that this is an outlier simulation, and have chosen to disregard it in the majority of our analysis. More work is needed to identify what causes the anomalous behavior of this simulation.

We have not considered the type of precipitation and, more specifically, how snowfall over the region will change in a warming climate. Using observations, Kunkel and et al. (2013) documented an increase in the frequency of extreme snowfall over the past several decades over the eastern U.S. It is not clear that this trend will persist over the entire region through the end of the century, as the occurrence of temperatures below the rain-snow transition



630 temperature may decrease (Diffenbaugh et al. 2013; O’Gorman 2014) despite the magnitude  
631 of extreme precipitation increasing during cold months (Figure 6). Given our results that  
632 show that the NEUS will experience the largest increases in extreme precipitation during  
633 the winter months, follow up studies on the detailed mechanisms of this increase and the  
634 type of precipitation falling during this time are required, and the NA-CORDEX ensemble  
635 may prove fruitful.

636 In summary, this work demonstrates that the entire NEUS should expect to have more  
637 frequent and more intense extreme precipitation events, with the largest increases in extreme  
638 precipitation occurring closest to the coast. Important open questions remain concerning the  
639 contribution of changes in Atlantic hurricanes to extreme precipitation over the NEUS, the  
640 type of precipitation that will fall during the heavier wintertime extreme precipitation events,  
641 and the dynamical changes which seem to damp the increases in extreme precipitation in  
642 projections of the 21st century. These questions may require novel modelling and analysis  
643 approaches to address. In any case, resilience and adaptation planners should prepare for  
644 a NEUS that experiences substantial increases in the frequency and intensity of extreme  
645 precipitation.

*Acknowledgments.* R. Nazarian, J. Vizzard, and C. Agostino gratefully acknowledge support from Fairfield University, including the College of Arts and Sciences, Science Institute, and Provost’s Office. R. Nazarian, J. Vizzard, and C. Agostino also gratefully acknowledge support from the NASA Connecticut Space Grant Consortium, award P-1704. N. Lutsko was supported by NSF grant OCE-2023483. The authors thank the editor and three reviewers for their helpful feedback, Seth McGinnis and Katja Winger for help accessing the NA-CORDEX data, and Kieran Bhatia for helpful comments on the presentation of the frequency analysis. More information about conducting undergraduate research with CORDEX can be found in Nazarian (2021).

*Data availability statement.* All NA-CORDEX simulations used in this study are freely available on the NCAR Climate Data Gateway: <https://www.earthsystemgrid.org/search/cordexsearch.html>.

## References

- Abbott, T., T. Cronin, and T. Beucler, 2020: Convective dynamics and the response of precipitation extremes to warming in radiative-convective equilibrium. *Journal of the Atmospheric Sciences*, **77**, 1637–1660.
- Agel, L., and M. Barlow, 2020: How well do cmip6 historical runs match observed northeast u.s. precipitation and extreme precipitation-related circulation? *Journal of Climate*, **33**, 9835–9848.
- Agel, L., M. Barlow, S. Feldstein, and W. Gutowski, 2018: Identification of large-scale meteorological patterns associated with extreme precipitation in the us northeast. *Climate Dynamics*, **50**, 1819–1839.
- Agel, L., M. Barlow, J. Polonia, and D. Coe, 2020: Simulation of northeast u.s. extreme precipitation and its associated circulation by cmip5 models. *Journal of Climate*, **33**, 9817–9834.

- 671 Agel, L., M. Barlow, J.-H. Qian, F. Colby, E. Douglas, and T. Eichler, 2015: Climatology of  
672 daily precipitation and extreme precipitation events in the northeast united states. *Journal*  
673 *of Hydrometeorology*, **16**, 2537–2557.
- 674 Alexander, L., and Coauthors, 2006: Global observed changes in daily climate extremes  
675 of temperature and precipitation. *Journal of Geophysical Research: Atmospheres*, **111**,  
676 D05 109.
- 677 Allen, M., and W. Ingram, 2002: Constraints on future changes in climate and the hydrologic  
678 cycle. *Nature*, **419**, 224–232.
- 679 Andrews, T., J. Gregory, M. Webb, and K. Taylor, 2012: Forcing, feedbacks and climate  
680 sensitivity in cmip5 couples atmosphere-ocean climate models. *Geophysical Research*  
681 *Letters*, **39**, L09 712.
- 682 Ashfaq, M., D. Rastogi, R. Mei, S.-C. Kao, S. Gangrade, B. Naz, and D. Touma, 2016:  
683 High-resolution ensemble projections of near-term regional climate over the continental  
684 united states. *Journal of Geophysical Research: Atmospheres*, **121**, 9943–9963.
- 685 Ban, N., J. Schmidli, and C. Schar, 2015: Heavy precipitation in a changing climate:  
686 does short-term summer precipitation increase faster? *Geophysical Research Letters*, **42**,  
687 1165–1172.
- 688 Bao, J., S. Sherwood, L. Alexander, and J. Evans, 2017: Future increases in extreme  
689 precipitation exceed observed scaling rates. *Nature Climate Change*, **7**, 128–132.
- 690 Behnke, R., S. Vavrus, A. Allstadt, T. Albright, W. Thogmartin, and V. Radeloff, 2016:  
691 Evaluation of downscaled, gridded climate data for the conterminous united states. *Eco-*  
692 *logical Applications*, **26**, 1338–1351.
- 693 Bukovsky, M., and L. Mearns, 2020: Regional climate change projections from na-cordex  
694 and their relation to climate sensitivity. *Climatic Change*, **162**, 645–665.

- Cannon, A., 2018: Multivariate quantile mapping bias correction: an n-dimensional probability density function transform for climate model simulations of multiple variables. *Climate Dynamics*, **50**, 31–49.
- Constantinidou, K., P. Hadjinicolaou, G. Zittis, and J. Lelieveld, 2020: Performance of land surface schemes in the wrf model for climate simulations over the mediterranean domain. *Earth Systems and Environment*, **4**, 647–665.
- Di Luca, A., R. de Elia, and R. Laprise, 2012: Potential for added value in precipitation simulated by high-resolution nested regional climate models and observations. *Climate Dynamics*, **38**, 1229–1247.
- Diffenbaugh, N., J. Pal, R. Trapp, and F. Giorgi, 2005: Fine-scale processes regulate the response of extreme events to global climate change. *Proceedings of the National Academy of Sciences*, **102**, 15 774–15 778.
- Diffenbaugh, N., M. Scherer, and M. Ashfaq, 2013: Response of snow-dependent hydrologic extremes to continued global warming. *Nature Climate Change*, **3**, 379–384.
- Fischer, E., U. Beyerle, and R. Knutti, 2013: Robust spatially aggregated projections of climate extremes. *Nature Climate Change*, **3**, 1033–1038.
- Fischer, E., J. Sedláček, E. Hawkins, and R. Knutti, 2014: Models agree on forced response pattern of precipitation and temperature extremes. *Geophysical Research Letters*, **41**, 8554–8562.
- Flato, G., J. Marotzke, B. Abiodun, P. Braconnot, S. Chou, W. Collins, and J. Zhang, 2014: Evaluation of climate models. *Climate change 2013 - the physical science basis: working group I contribution to the fifth assessment report of the intergovernmental panel on climate change*, Cambridge University Press, 741–866.
- Frei, A., K. Kunkel, and A. Matonse, 2015: The seasonal nature of extreme hydrological events in the northeastern united states. *Journal of Hydrometeorology*, **16**, 2065–2085.

- 720 Gandini, A., L. Garmendia, I. Alvarez, and J.-T. San-Jose, 2020: A holistic and multi-  
721 stakeholder methodology for vulnerability assessment of cities to flooding and extreme  
722 precipitation events. *Sustainable Cities and Society*, **63**, 102 437.
- 723 Garner, A., R. Kopp, and B. Horton, 2021: Evolving tropical cyclone tracks in the north  
724 atlantic in a warming climate. *Earth's Future*, e2021EF002326.
- 725 Groisman, P., R. Knight, D. Easterling, T. Karl, G. Hegerl, and V. Razuvaev, 2005: Trends  
726 in intense precipitation in the climate record. *Journal of Climate*, **18**, 1326–1350.
- 727 Hausfather, Z., and G. Peters, 2020: Rcp8.5 is a problematic scenario for near-term emis-  
728 sions. *Proceedings of the National Academy of Sciences*, **117**, 27 791–27 792.
- 729 Hayhoe, K., and Coauthors, 2008: Regional climate change projections for the northeast  
730 usa. *Mitigation and Adaptation Strategies for Global Change*, **13**, 425–436.
- 731 Hoerling, M., J. Eischeid, J. Perlwitz, X.-W. Quan, K. Wolter, and L. Cheng, 2016: Char-  
732 actterizing recent trends in u.s. heavy precipitation. *Journal of Climate*, **29**, 2313–2332.
- 733 Howarth, M., C. Thorncroft, and L. Bosart, 2019: Changes in extreme precipitation in the  
734 northeast united states: 1979-2014. *Journal of Hydrometeorology*, **20**, 673–689.
- 735 Huang, H., C. Patricola, J. Winter, E. Osterberg, and J. Mankin, 2021: Rise in northeast  
736 us extreme precipitation caused by atlantic variability and climatte change. *Weather and*  
737 *Climate Extremes*, **33**, 100 351.
- 738 Huang, H., J. Winter, and E. Osterberg, 2018: Mechanisms of abrupt extreme precipittation  
739 change over the northeastern united states. *Journal of Geophysical Research: Atmo-*  
740 *spheres*, **123**, 7179–7192.
- 741 Huang, H., J. Winter, E. Osterberg, R. Horton, and B. Beckage, 2017: Total and extreme  
742 precipitation changes over the northeastern united states. *Journal of Hydrometeorology*,  
743 **18**, 1783–1798.

- Ivancic, T., and S. Shaw, 2016: A u.s.-based analysis of the ability of the clausius-clapeyron relationship to explain changes in extreme rainfall with changing temperature. *Journal of Geophysical Research: Atmospheres*, **121**, 3066–3078.
- Kao, S.-C., and A. Ganguly, 2011: Intensity, duration, and frequency of precipitation extremes under 21st-century warming scenarios. *Journal of Geophysical Research: Atmospheres*, **116**, D16 119.
- Karmalkar, A., 2018: Interpreting results from the narccap and na-cordex ensembles in the context of uncertainty in regional climate change projections. *Bulletin of the American Meteorological Society*, **99**, 2093–2106.
- Kharin, V., F. Zwiers, and M. Wehner, 2013: Changes in temperature and precipitation extremes in the cmip5 ensemble. *Climatic Change*, **119**, 345–357.
- Kirchmeier-Young, M., F. Zwiers, N. Gillett, and A. Cannon, 2017: Attributing extreme fire risk in western canada to human emissions. *Climatic Change*, **144**, 365–379.
- Kirschbaum, D., R. Adler, D. Adler, C. Peters-Lidard, and G. Huffman, 2012: Global distribution of extreme precipitation and high-impact landslides in 2010 relative to previous years. *Journal of Hydrometeorology*, **13**, 1536–1551.
- Knist, S., and coauthors, 2017: Land-atmosphere coupling in euro-cordex evaluation experiments. *Journal of Geophysical Research: Atmospheres*, **122**, 79–103.
- Kocin, P., and L. Uccellini, 2004: *Northeast snowstorms*. American Meteorological Society.
- Kunkel, K., and et al., 2013: Monitoring and understanding trends in extreme storms: state of knowledge. *Bulletin of the American Meteorological Society*, **94**, 499–514.
- Langhans, W., K. Yeo, and D. Romps, 2015: Lagrangian investigation of the precipitation efficiency of convective clouds. *Journal of the Atmospheric Sciences*, **72**, 1045–1062.
- Leung, L., L. Mearns, F. Giorgi, and R. Wilby, 2003: Regional climate research: needs and opportunities. *Bulletin of the American Meteorological Society*, **84**, 89–95.

- 769 Lopez-Cantu, T., A. Prein, and C. Samaras, 2020: Uncertainties in future u.s. extreme  
770 precipitation from downscaled climate projections. *Geophysical Research Letters*, **47**,  
771 e2019GL086797.
- 772 Lucas-Picher, P., R. Laprise, and K. Winger, 2016: Evidence of added value in north  
773 american regional climate model hindcast simulations using ever-increasing horizontal  
774 resolutions. *Climate Dynamics*, **48**, 2611–2633.
- 775 Lutsko, N., and T. Cronin, 2018: Increase in precipitation efficiency with surface warming  
776 in radiative-convective equilibrium. *Journal of Advances in Modeling Earth Systems*, **10**,  
777 2992–3010.
- 778 Martinez-Villalobos, C., and J. Neelin, 2019: Why do precipitation intensities tend to follow  
779 gamma distributions? *Journal of the Atmospheric Sciences*, **76**, 3611–3631.
- 780 McGinnis, S., and L. Mearns, 2021: Building a climate service for north america based on  
781 the na-cordex data archive. *Climate Services*, **22**, 100233.
- 782 Muller, C., and Y. Takayabu, 2020: Response of precipitation extremes to warming: what  
783 have we learned from theory and idealized cloud-resolving simulations, and what remains  
784 to be learned? *Environmental Research Letters*, **15**, 035001.
- 785 Myhre, G., and Coauthors, 2019: Frequency of extreme precipitation increases extensively  
786 with event rareness under global warming. *Scientific Reports*, **9**, 16063.
- 787 Nazarian, R., 2021: The use of model intercomparison projects in engaging undergraduates  
788 in climate change research. *Scholarship and Practice of Undergraduate Research*, **5**,  
789 27–28.
- 790 Ning, L., E. Riddle, and R. Bradley, 2015: Projected changes in climate extremes over the  
791 northeastern united states. *Journal of Climate*, **28**, 3289–3310.
- 792 Nishant, N., and S. Sherwood, 2021: How strongly are mean and extreme precipitation  
793 coupled? *Geophysical Research Letters*, **48**, e2020GL092075.

- 794 O’Gorman, P., 2014: Contrasting responses of mean and extreme snowfall to climate  
795 change. *Nature*, **512**, 416–418.
- 796 O’Gorman, P., 2015: Precipitation extremes under climate change. *Current Climate Change*  
797 *Reports*, **1**, 49–59.
- 798 Pendergrass, A., and E. Gerber, 2016: The rain is askew: two idealized models relating  
799 vertical velocity and precipitation distributions in a warming world. *Journal of Climate*,  
800 **29**, 6445–6462.
- 801 Pendergrass, A., F. Lehner, B. Sanderson, and Y. Xu, 2015: Does extreme precipitation  
802 intensity depend on the emission scenario? *Geophysical Research Letters*, **42**, 8767–  
803 8774.
- 804 Pendergrass, A., K. Reed, and B. Medeiros, 2016: The link between extreme precipi-  
805 tation and convective organization in a warming climate: global radiative-convective  
806 equilibrium simulations. *Geophysical Research Letters*, **43**, 11 445–11 452.
- 807 Pithan, F., and T. Mauritsen, 2014: Arctic amplification dominated by temperature feedbacks  
808 in contemporary climate models. *Nature Geoscience*, **7**, 181–184.
- 809 Rastogi, D., D. Touma, J. Evans, and M. Ashfaq, 2020: Shift toward intense and widespread  
810 precipitation events over the united states by mid-21st century. *Geophysical Research*  
811 *Letters*, **47**.
- 812 Rawlins, M., R. Bradley, and H. Diaz, 2012: Assessment of regional climate model sim-  
813 ulation estimates over the northeast united states. *Journal of Geophysical Research:*  
814 *Atmospheres*, **117**, D23 112.
- 815 Rendfrey, T., M. Bukovsky, R. McCrary, and R. Fuentes-Franco, 2021: An assessment  
816 of tropical cyclones in north american cordex wrf simulations. *Weather and Climate*  
817 *Extremes*, **34**, 100 382.



- 818 Rosenzweig, C., F. Tubiello, R. Goldberg, E. Mills, and J. Bloomfield, 2002: Increased crop  
819 damage in the us from excess precipitation under climate change. *Global Environmental*  
820 *Change*, **12**, 197–202.
- 821 Schar, C., and Coauthors, 2016: Percentile indices for assessing changes in heavy precipi-  
822 tation events. *Climatic Change*, **137**, 201–216.
- 823 Schwalm, C., S. Glendon, and P. Duffy, 2020: Rcp8.5 tracks cumulative co2 emissions.  
824 *Proceedings of the National Academy of Sciences*, **33**, 19 656–19 657.
- 825 Sheffield, J., and Coauthors, 2013: North american climate in cmip5 experiments. part 1:  
826 evaluation of historical simulations of continental and regional climatology. *Journal of*  
827 *Climate*, **26**, 9209–9245.
- 828 Sillmann, J., V. Kharin, F. Zwiers, X. Zhang, and Z. Brunaugh, 2013: Climate extremes  
829 indices in the cmip5 multimodel ensemble: part 2. future climate projections. *Journal of*  
830 *Geophysical Research: Atmospheres*, **118**, 2473–2493.
- 831 Singh, J., S. Karmakar, D. PaiMazumder, S. Ghosh, and D. Niyogi, 2020: Urbanization  
832 alters rainfall extremes over the contiguous united states. *Environmental Research Letters*,  
833 **15**.
- 834 Singh, M., and P. O’Gorman, 2014: Influence of microphysics on the scaling of precipitation  
835 extremes with temperature. *Geophysical Research Letters*, **41**, 6037–6044.
- 836 Soares, P., J. Careto, R. Cardoso, K. Goergen, and R. Trigo, 2019: Land-atmosphere  
837 coupling regimes in a future climate in africa: from model evaluation to projections  
838 based on cordex-africa. *Journal of Geophysical Research: Atmospheres*, **124**, 11 118–  
839 11 142.
- 840 Steinschneider, S., and N. Najibi, 2022: Observed and projected scaling of daily extreme  
841 precipitation with dew point temperature at annual and seasonal scales across the northeast  
842 united states. *Journal of Hydrometeorology*, **23**, 403–419.

843 Tabari, H., 2020: Climate change impact on flood and extreme precipitation increases with  
844 water availability. *Scientific Reports*, **10**, 13 768.

845 Tamarin-Brodsky, T., and O. Hadas, 2019: The asymmetry of vertical velocity in current  
846 and future climate. *Geophysical Research Letters*, **46**, 374–382.

847 Thibeault, J., and A. Seth, 2014: Changing climate extremes in the northeast united states:  
848 observations and projections from cmip5. *Climatic Change*, **127**, 273–287.

849 Walsh, J., and Coauthors, 2014: *Our Changing Climate. Climate Change Impacts in the*  
850 *United States: The Third National Climate Assessment*, chap. 2, 19–67. U.S. Global  
851 Change Research Program.

852 Wang, G., C. Kirchhoff, A. Seth, J. Abatzoglou, B. Livneh, D. Pierce, L. Fomenko, and  
853 T. Ding, 2020: Projected changes of precipitation characteristics depend on downscaling  
854 method and training data: Maca versus loca using the u.s. northeast as an example.  
855 *Journal of Hydrometeorology*, **21**, 2739–2758.

856 Wilhelmi, O., and R. Morss, 2013: Integrated analysis of societal vulnerability in an extreme  
857 precipitation event: a fort collins case study. *Environmental Science & Policy*, **26**, 49–62.

858 Zarzycki, C., 2018: Projecting changes in societally impactful northeastern u.s. snowstorms.  
859 *Geophysical Research Letters*, **45**, 12 067–12 075.

860 Zscheischler, J., and Coauthors, 2018: Future climate risk from compound events. *Nature*  
861 *Climate Change*, **8**, 469–477.